Influence of foundation type on seismic response of low-rise structures in liquefiable soil

Qi, Shengwenjun; Knappett, Jonathan

Published in:
Soil Dynamics and Earthquake Engineering

DOI:
10.1016/j.soildyn.2019.105786

Publication date:
2020

Document Version
Peer reviewed version

Influence of foundation type on seismic response of low-rise structures in liquefiable soil

Qi, S.[1] and Knappett, J.A.[2*]

[1] *PhD student, University of Dundee, Dundee, DD1 4HN, UK*

[2] *Professor of Civil Engineering, University of Dundee, Dundee, DD1 4HN, UK,*

[*] *Corresponding author: +44-1382-384345, j.a.knappett@dundee.ac.uk*

Highlights:

1. Structure-soil-structure interaction (SSSI) is investigated in liquefiable soil.
2. Empirical method for estimating peak surface motion in partially liquefied soil.
3. Raft foundations lower structural demands compared to strips during SSSI.
4. Reduced demand associated with increased post-earthquake foundation deformations.
5. Foundation effects are apparent in mainshock and aftershocks.

Influence of foundation type on seismic response of low-rise structures in liquefiable soil

Qi, S.[1] and Knappett, J.A.[2*]

[1] *PhD student, University of Dundee, Dundee, DD1 4HN, UK*

[2] *Professor of Civil Engineering, University of Dundee, Dundee, DD1 4HN, UK,*

[*] *Corresponding author: +44-1382-384345, j.a.knappett@dundee.ac.uk*

Abstract

The 2010-2011 Canterbury Earthquake Sequence (CES) caused extensive damage to low-rise structures in the city of Christchurch, New Zealand, mainly due to liquefaction-induced effects including settlement and angular distortion. This paper will present the results of dynamic centrifuge tests comparing the effects of liquefaction on the seismic performance of isolated structures with different types of shallow foundations (strips or a raft), and the effect of being situated adjacent to a heavier neighbouring structure of the same foundation type (i.e. considering structure-soil-structure interaction, SSSI). Performance will be evaluated under a sequence of successive earthquakes from the 2010-2011 CES and 2011 Tohoku Earthquake, Japan, to permit study under ground motions and aftershocks generating full liquefaction either extensively or to only a limited depth below ground level. The results show firstly that lower intensity ground shaking occurs at the ground surface when liquefaction occurs and that this can be estimated as a function of the degree of liquefaction using a simple estimation method. When subjected to these ground motions, using strip foundations for isolated structures can result in a reduction in structural demand, especially when the soil is extensively liquefied. When a neighbouring structure with the same foundation type is present, the effects of SSSI within liquefied soil result in changes to natural period and damping such that raft-founded structures exhibited lower

structural demands. In either case (isolated or adjacent), a reduction in structural demand is accompanied by an increase in post-earthquake permanent foundation deformation.

1 Introduction

Due to increasing urbanisation and population growth in recent decades, the interaction between adjacent structures in urban area during earthquakes is becoming of greater concern than their behaviour when they are isolated. Clear evidence of SSSI was first observed in the 1987 Whittier-Narrows (California) Earthquake from field observations of the response of two adjacent seven-storey buildings on moderately dense to dense granular soil [1]. Closely spaced structures may also be founded on soils which are liquefiable. The reduction in soil strength and degradation in shear stiffness occurring due to excess pore water pressure (EPWP) build-up is often a major cause of excessive settlement and angular distortion for buildings on shallow foundations during earthquakes in urban areas, with numerous examples having been observed in the 2010-2011 Canterbury Earthquake Sequence in New Zealand (e.g. [2]).

Previous early numerical studies of SSSI (e.g. [3,4]) investigated multiple rigid block interaction on a linear elastic subgrade representative of the stiffness of soil to model a highly idealised urban area and studied the dynamic characteristics, (particularly associated with natural periods of vibration) associated with the groups of structures. Further studies in [5] used 1-g shaking table tests of more representative equivalent single-degree-of-freedom oscillators on a linear elastic subgrade, considering two adjacent buildings. This work has suggested that the relative dynamic properties (natural periods) of the individual structures could result in either an increase or decrease of the peak acceleration and spectral power by large amount. This data was used to validate an analytical model [6] that identifies not only vibrational dynamic characteristics of grouped structures, but also, the resulting (elastic) structural response. To improve upon previous linear-elastic idealisations of soil, centrifuge testing has also previously been conducted to investigate the behaviour of single and adjacent (paired) structures on non-liquefiable (but non-linear) soil [7] which showed structural response effects consistent with [5], and also introduced the effects of SSSI on foundation response in terms of permanent post-earthquake settlement and rotation (tilt caused by differential settlement). Although these studies have provided very useful insights into SSSI none have previously considered how the interaction may change in the presence of soil liquefaction, despite extensive study of individual shallow foundation behaviour on liquefiable soil (e.g. [8,9]).

This study aims to build on this previous work by considering: (i) the effect of liquefaction on the soil-structure interaction behaviour of an isolated multi-degree-of-freedom structure having one of two types of shallow foundations (individual strips or a one-piece raft) within liquefiable granular soil; and (ii) how this behaviour is modified by SSSI due to the presence of a nearby (dissimilar) structure. The results from four multi-event centrifuge tests are presented in this study. In the tests, a series of consecutive earthquake ground motions measured at a single site from the 2010-2011 Canterbury Earthquake Sequence was considered to observe performance under a strong earthquake and weaker aftershock motions, followed by a long duration high intensity 'double pulse' motion from the 2011 Tohoku Earthquake which could potentially apply large accelerations (and therefore large inertial forces) into the structure(s) in the second pulse of high acceleration after liquefaction had been triggered by the first.

2 Centrifuge modelling

The centrifuge tests presented herein were conducted using models at 1:40 scale, tested at 40-*g* centrifugal acceleration using the Actidyn Systèmes C67 3.5 m radius beam centrifuge facility at the University of Dundee, UK. All parameters herein are presented at prototype scale unless otherwise stated. Scaling laws used to determine model parameters from prototype values for centrifuge modelling can be found in [10, 11].

2.1 Model structures

In the 2011 Christchurch Earthquake, 80% of the heavily damaged buildings in the Central Business District (CBD) were one or two-storey buildings founded on shallow foundations [12]. This type of buildings is the most common in urban areas, while being the least likely to have extensive seismic detailing (compared to high value, high-rise structures in a CBD). The design of prototype structures was not to replicate a specific actual building but to retain key characteristics of low-rise buildings which were two-storey, single bay, moment resisting frames with concrete slab floors sitting on either a square raft or separated strip concrete foundations. The storey height (3 m) and floor area 3.6 m× 3.6 m were representative of low-rise buildings, accounting also for the space constraints in the centrifuge. The model frames consisted of four individual square columns machined from solid 6082-series aluminium alloy rods interconnected by two floor slabs fabricated from aluminium plates.

In the case of adjacent structures, an increase in slab mass by 44% was made to one of the structures (which otherwise had structural frame elements of the same stiffness) resulting in a 20% lengthening of natural period T_n. This arrangement of dissimilar structures was selected as this difference in natural period between adjacent buildings was observed to produce the greatest influence of SSSI for linear elastic ground behaviour by [5]. It may also be thought of as representative of a case where one structure from a pair of initially identical structures has had a change of use (increasing the slab loading). Additional thin steel plates were bolted to the model slabs to achieve the mass difference between the two structures in the adjacent cases. The foundation edge-to-edge spacing was 1.2 m at prototype scale which was 1/3 of the structural bay width and 1/4 of total building width including the foundations, to enable strong SSSI effects [13-15] while avoiding any building pounding and instrument damage during experiments. A summary of test configurations is provided in Table 1.

The raft foundation was made of a single aluminium alloy plate due to the similarity in density between this material and reinforced concrete (2700 kg/m^3 versus 2400 kg/m^3, respectively), which was 4.8 m × 4.8 m square in area with a high static factor of safety (*FOS*) against bearing failure on the fully saturated medium dense sandy soil used (see later) due to the large area. The strip foundations were made of the same material but separated on two sides of the structure (i.e. each supporting two columns) being B = 1.2 m in width and L = 4.8 m in length (B/L = 4), providing a static *FOS* of 3 or 2.5 for the ‘light’ and ‘heavy’ building cases. The raft foundation had the same external footprint, but with solid material infilling between the strip foundations. Both types of foundations satisfied static requirements at the ultimate limiting state. The bearing capacities of the strip and raft foundations are shown in Table 2 following design method presented in [16]. The presence of an adjacent structure on strip foundations given the foundation edge-to edge spacing of 1.2 m was not expected to affect the bearing capacity at ultimate limit state compared to a building in isolation [16, 17], however, it would have an effect on initial settlements and tilt of the structures under static conditions (both for strip and raft foundations). An adjacent building with a raft foundation was expected to increase the bearing capacity of its neighbour by a factor of 1.5 [16, 17]. The structure on the raft foundation in isolation was expected to resist a maximum seismic action $a_g = 0.44g$ in the absence of liquefaction based on conventional seismic bearing capacity approaches [18]; for the structure on strip foundations this value was $0.23g$. All foundations were coated on the base and sides with a thin layer of the subsoil using an epoxy resin to approximate the rough soil-footing interface between soil and concrete cast in-situ. Figure 1 shows the instrumented model structure on strip foundations with dimensions at prototype and model scales.

A typical fundamental natural period (T_n) of a prototype two-storey structure was approximated using Equation 1 [19]:

$$T_n = 0.1N \tag{1}$$

where N is the number of stories of the structure ($N = 2$ in this case) and T_n is in seconds.

The mass of each floor slab was set to be the same ($M_1 = M_2$) and determined based on a 3.6 m × 3.6 m × 0.5 m thick reinforced concrete slab. The equivalent single-degree-of-freedom stiffness of the structure in the fundamental mode (K_{eq}) was then determined from Equation 2:

$$T_n = 2\pi\sqrt{\frac{M_{eq}}{K_{eq}}} \tag{2}$$

where:

$$\mathrm{M_{eq}} = \mathrm{M_1}\,\overline{\mathrm{y_1}}^2 + \mathrm{M_2}\,\overline{\mathrm{y_2}}^2 \tag{3}$$

$$K_{eq} = K_1(\overline{y_1})^2 + K_2(\overline{y_2} - \overline{y_1})^2 \tag{4}$$

The normalized modal coordinates associated with the fundamental mode were $\bar{y}_1 = 0.45$ and $\bar{y}_2 = 0.89$, based on an eigenvalue analysis for the two-storey structure having equal lateral stiffness and mass at each storey. By setting the four columns in each storey to have the same lateral stiffness,

k_{col} (i.e. k_{col} = 0.25K_1 = 0.25K_2), and selecting the closest available steel Universal Column size to provide sufficient bending stiffness EI (UC 203×203×86), the natural period of the light structure was finally 0.21 s and that of the heavier structure 0.25 s. A summary of section properties is provided in Table 2.

2.2 Model preparation and soil properties

For all tests presented herein, a single set of medium dense soil properties was used. Dry HST95 Congleton silica sand at a relative density of I_D = 55%-60% and 8 m depth at prototype scale was initially air-pluviated into an Equivalent Shear Beam (ESB) container, then saturated using hydroxypropyl methyl-cellulose (HPMC) pore fluid with a viscosity 40 times higher than water. This was required to ensure the time scales for seepage and inertial effects were consistent with prototype values, which is further discussed in [20]. Details of the performance of viscous pore fluids in dynamic centrifuge testing can be found in [21]. Saturation was conducted by allowing the fluid to enter the model under a constant head through orifices in the bottom of the ESB container at a relatively low flow rate until it reached a level 2 mm above the model surface (to ensure that the soil would remain fully saturated even if there was ground heave adjacent to the foundations).

The ESB container consisted of stacked aluminium rings separated by thin rubber layers, with the aim of providing flexible boundaries that deform similarly to the fundamental mode of the soil to minimise boundary effects. The designed natural frequency of the container used was 2 Hz at prototype scale for a horizontal acceleration coefficient k_h = 0.4 at 50-g [22, 23]. Detailed discussion of all of the design and performance requirements for such a container can be found in [24-26]. Physical properties of the HST95 sand are listed in Table 3 after [27]. In the absence of liquefaction, the ground profile so modelled represented ground type E according to Eurocode 8 [28].

The soil was instrumented with accelerometers and pore pressure transducers (PPT) at five different depths in isolated tests and 3 depths in adjacent tests. Figure 2 shows the instrumentation details of Tests SQ04 and SQ07 as examples (instrument positions are denoted by letters for SQ04). ADXL-78 single-axis micro-electromechanical system (MEMS) accelerometers were used to measure ground motions and infer stress-strain behaviour and both HM-91 PPTs and PDCR-81 PPTs were used to measure the generation and dissipation of EPWP. Soil measurements were made close to the input 'bedrock' (point E), at a vertical array in the free-field (Points A-E), and below each building at similar depths to free-field points (Points F-G). The structures were also instrumented with the same type of accelerometers (see Figures 1 and 2) to measure the vertical and horizontal dynamic motions at the foundations and horizontal motions at each storey (Points H to K). The storey acceleration was derived from a high pass zero-phase-shift filtering of horizontal accelerometers attached on the structures (Points J and K in Figure 2), to remove any monotonic component due to permanent deformation. The cyclic sway (= inter-storey drift + lateral displacement due to rotation) was derived by double integration of the storey acceleration data. The dynamic inter-storey drift was then determined by removing the cyclic rotational component measured from the vertical foundation accelerometers. Horizontal Linear variable Differential Transformers (LVDTs) were avoided for deriving cyclic-sway and inter-storey drift as the individual floors were 6 mm thick at model scale and there was initial settlement during spin-up of the centrifuge which may have resulted in the horizontal LVDTs losing contact with the floors. As the response of the structures was elastic, the accelerometer approach outlined above was adopted instead.

After loading the saturated soil model onto the centrifuge, the isolated or adjacent structures were placed on the soil surface to be nominally level, following which any initial tilt was recorded using a clinometer to provide a baseline for subsequent measurements of structural rotation. An overhead gantry was then placed above the structures on either side allowing the placement of linear variable differential LVDTs to measure permanent settlement and rotation of the structures, and settlement of the soil surface above the free-field array. Due to the small vertical cyclic displacements of the foundations, the gross settlements and rotations of the foundations were derived from superposing low-pass zero-phase shift eighth-order Butterworth filtered LVDT data (cut-off frequency 0.75 Hz in prototype) to provide the monotonic component and high-pass zero-phase shift eighth-order Buterworth filtered (cut-off frequency of 1.5 Hz in prototype) double integrated vertical accelerometer data to provide the dynamic component. The gross settlement was derived by averaging the compound LVDT data for the two instruments on each side of an individual structure. Rotation was derived by the difference of the two compound LVDT traces divided by the width of structure, with rotation to the right as shown in Figure 2 being positive.

2.3 Ground motions

Following spin-up to 40-g, a re-ordered sequence of motions from the Canterbury Series of 2010-2011 (Christchurch, New Zealand) recorded at the Christchurch Botanical Gardens Station was applied, followed by a long duration 'double-pulse' motion from the 2011 Tohoku Earthquake (Japan) recorded at the Ishinomaki Station. The Christchurch earthquake of February 2011 was chosen to be the first motion, aiming to induce full liquefaction with the initial condition of the soil fully known (no pre-shaking). Three subsequent less intense aftershocks ('June13a' from June 2011, the Darfield earthquake of 2010 and 'June13b', also from 2011) were subsequently applied which were expected to produce progressively lower EPWP generation, representing various partially-liquefied conditions. The Tohoku motion was applied last with the aim of fully re-liquefying the soil following the previous sequence of motions during the initial pulse of high peak ground acceleration (PGA) followed by a second high PGA pulse while the soil remained in a liquefied state to simulate a potentially extreme load case for the structure(s). Each motion was applied recording the response of all instruments at 4 kHz sampling frequency for 4 minutes at model scale (160 minutes at prototype scale) following the end of shaking to ensure that the EPWP observed from the PPTs returned to zero and the building was stationary before applying the subsequent motion.

The motions were applied using the Actidyn QS67-2 servo-hydraulic earthquake simulator (EQS) at the University of Dundee. Details of its performance may be found in [23,29]. Motions were filtered using an eighth order Butterworth filter with a pass range between 2.3-7.5 Hz (at prototype scale). The nominal 5% damped response spectra of the recorded input motions are shown in Figure 3. The fixed-base natural period of the light structure $T_n = 0.21s$) is also shown which falls within the rising phase of the spectra. It was observed that the first and last motion have similar spectral response at a fixed-base period of 0.21s indicating that these two motions were expected to result in similar peak structural response in the absence of any soil-structure interaction (SSI), while being of very different duration. The effects of SSI on period lengthening will be discussed from measured data later. The repeatability of input motions across the four centrifuge tests (essential for valid test-to-test comparisons) is demonstrated in Figure 4 in terms of normalised spectra, in which the Type 1 elastic design response spectrum (behaviour factor *q*=1 and Ground type A for consistency with the input motions being at 'bedrock' level) from Eurocode 8 for earthquakes with surface-wave magnitude greater than 5.5 is also shown for context [28].

3 Results

3.1 Free field soil response

Data showing peak EPWP generation in the free field are presented in Figure 5 in terms of the normalised ratio r_u (equal to EPWP divided by initial vertical effective stress). Actual pre-shaking depths of the PPTs were determined based on the static pore pressures measured during spin-up of the centrifuge and these were used in place of the nominal values shown in Figure 2 for EQ1. Thereafter, PPT positions were corrected for any floating or sinking between earthquake events based on any final (small) static offsets in measurements after EPWP had fully dissipated (i.e. $dr_u/dt = 0$).

Liquefaction susceptibility/triggering analyses were also conducted following the approach of [30]. The factor of safety against liquefaction (F_{SL}), determined using Equation 5, is shown in Figure 5(a) (as cross markers connected with dashes lines)

$$F_{sL} = \frac{CRR}{CSR} \quad (5)$$

where *CRR* = Cyclic Resistance Ratio and *CSR* = Cyclic Stress Ratio. The *CRR* value was determined for EQ1 using an estimated equivalent normalised SPT blowcount $(N_1)_{60}$ of 22 determined using Equation 6, which is a reasonable estimation for most aged natural deposits in terms of I_D [16,31].

$$(N_1)_{60}/{I_D}^2 \approx 60 \quad (6)$$

where $I_D = 60\%$. The *CSR* value was determined based on the ground motion according to [30] and input bedrock PGA in the free-field assuming linear change with height to a value at the surface giving an amplification factor of 1.4 (soil factor for ground type E in EC8) in the absence of any liquefaction effect.

Adopting methods described in [32], the peak pore pressure ratio with depth was estimated. This assumes that when $F_{sL} \leq 1$, full liquefaction existed and the peak EPWP was equal to the initial effective vertical effective stress at that depth ($r_{u,predicted}$=1). Once F_{sL} >1, the peak EPWP was assumed to be thereafter constant with depth, providing a bi-linear approximation to an EPWP isochrone for the time when maximum EPWP is reached. Dividing this constant EPWP by the increasing vertical effective stress with depth gave a reducing profile of r_u with depth shown by the solid lines in Figure 5(a).

Figure 5(b) shows the measured peak $r_{u,FF}$ at each depth from all tests and events. Variations in $r_{u,FF}$ between tests was thought to be caused by (i) individual local variations of density between soil models from model preparation, which are unavoidable; and/or (ii) the influence of the nearby structures. Although the position of the free-field instrumentation was kept at least 100 mm from the wall of the ESB container, 100 mm (3.3*B* strip 0.8*B* raft) from the model structures in the adjacent cases, and 180 mm (6.0*B* strip 1.5*B* raft) in the isolated cases, the free-field EPWP of isolated raft and all adjacent cases were all lower than in the isolated strip case, where the foundation-free-field spacing was largest (6*B*). The free-field instruments in the isolated strip case therefore represented the best approximation to true free-field conditions.

In EQ1 (Christchurch Earthquake) under virgin initial soil conditions the soil experienced full liquefaction over all depths, consistent with F_{sL} < 1 everywhere. In EQ2 and EQ5 (Tohoku Earthquake) extensive liquefaction was also achieved as suggested by F_{sL} <1 everywhere, even with the initial conditions of the soil having been altered by the previous shaking (e.g. resulting in densification, particularly near-surface). In the weakest of these three motions (EQ2) full liquefaction was only achieved within the upper half of the soil layer (which would likely be deep enough to lead to similar structural response as in EQ1 and EQ5, given that the foundations are shallow). Figure 6 demonstrates that the effects of full liquefaction to full/half depth resulted in substantial reductions in motion from the bedrock input motion (isolated strip case shown), as the shear waves were not ale to amplify as they propagated due to the low shear strength of the soil in the fully liquefied state which limited transfer of shear stress.

The smaller aftershocks (EQ3 and EQ4) had significantly lower PGA (< 0.2-g) compared to the other motions (PGA > 0.3-g) and these also grouped together with similar behaviour, exhibiting full liquefaction only at the very shallowest locations in Figure 5 (b). The estimated r_u profiles from Figure 5(a) can also be seen to provide a reasonable upper-bound to the measured data (i.e. conservative for use in design). From Figure 6 this 'surficial liquefaction' resulted in approximately no reduction in motion amplitude at the ground surface (i.e. reduction in ground motion attenuation due to only partial liquefaction) in both cases, consistent with the similarity in r_u profiles. In these cases, the deeper soils allowed motions to partially amplify as the shear waves travelled upwards, before being attenuated by the low strength liquefied surface layers. As shown in Figure 7, the attenuation in PGA of EQ3 and EQ4 was shallower (3.5 m below surface, consistent with the depth of full liquefaction from Figure 5).

Figure 8 shows the transfer function required to convert the spectra of the input motion at bedrock to the corresponding free-field surface values in Figure 8 (i.e. the soil amplification factor – S in EC8; BSI, 2005). The limiting values at low (T<0.4s) and high (T>0.8s) periods are further plotted in Figure 9 together with S = 1.4 (for ground type E) for the case of no liquefaction (r_u=0, everywhere). The values are limited to only isolated cases as the free field was less affected by the presence of the structures in these cases and thus better represents the true free-field condition. This is plotted against a parameter representing the area beneath the r_u-depth curve, normalised by layer depth, which is a measure of the cumulative amount of liquefaction within the soil. A value of 1.0 indicates that all of the soil is fully liquefied (i.e. at all depths). With the exception of one datapoint, a negative trend can be observed from the experimental data which is consistent with the amplification factor being 1.4 when there is no liquefaction. Two trendlines can be drawn by least-squares regression for structures of period T<0.4 s and T>0.8 s implying the potential reductions for a wide period range of structures and interpretation can be made between the two trendlines.

3.2 Response of isolated structures with different foundation types

3.2.1 Response in fully-liquefied soil

This section will focus on structural demand for storey 1 only, as this storey exhibited the largest deformation (inter-storey drift) and was also close to the centre of mass of the two-storey structure. The time histories of structural response for strip foundations (black line) and raft foundation (grey line) during EQ1 (full liquefaction, virgin soil) and EQ5 (full liquefaction, pre-shaken soil) are shown in Figures 10 and 11, respectively. It is shown that strip foundations minimised transmission of accelerations to the structure in each (isolated) case (Figures 10(a) and 11(a)).

The free field settlement recorded from the LVDT at the free-field surface in the isolated strip case is shown for reference in Figure 10 (b) and Figure 11(b). This test had the most representative free-field condition at the location of the transducer and only a single case is shown for clarity. The initial settlement in spinning-up the centrifuge from 1g to 40g is shown as the starting settlement prior to EQ1. The initial structural tilt caused by the spin-up is also shown as the starting value of EQ1 in Figure 10 (c). Comparing the structural and free field settlements in the isolated strip case, the initial settlement during spin-up of the structure was much larger than that in the free-field due to the applied foundation bearing pressure.

In Figure 10 (b) and (c) for EQ1, the building settlement and rotation of the isolated raft and strip were largely similar. By EQ 5 (Figure 11 (b) and (c)) the post-earthquake rotation of the structure with strip foundations had increased significantly, together with greater accumulated settlement prior to EQ5 and larger increases in settlement during EQ5. This demonstrates that any benefit of strip foundations in protecting the structure by minimising transmitted accelerations in fully-liquefied soil comes at a price of greater post-earthquake foundation deformation. This is similar to the trade-off between settlement and structural protection in rocking-isolated structures [e.g. 33].

3.2.2 'Double pulse' excitation behaviour

The Tohoku Earthquake (EQ5) is shown divided into two regions in Figure 11, separated by a dashed line. In the first part, the largest ground accelerations occured when the soil was still liquefying, while in the second part, similarly large input ground accelerations occured when the soil was already fully liquefied (Figure 11(d)). The cycles of EPWP generation of the r_u time history in Figure 10 (d) and Figure 11 (d) were filtered out due to an unexpected band frequency of noise that was superimposed on the signal for these instruments within the frequency range of the earthquakes. As a result, the values shown indicate the monotonic component of the EPWP. The effect of the different r_u values at these two different instances were reflected in the size of the storey accelerations, which were larger during the first part when $r_u < 1$ and smaller in the second part when $r_u = 1$. The maximum ratios of storey acceleration in the strip foundation compared to the raft foundation in EQ5 were 0.7 for $r_u < 1$ and 0.52 for $r_u = 1$ (Figure 11 (a)). Such large reductions of structural response due to SSI may outweigh the negative effects of additional settlement (+25%), making separated strip foundations desirable over rafts in liquefiable soil for isolated structures. In the second part of the motion, there was also greater earthquake-induced permanent rotation of raft foundations compared to strips, but post-earthquake rotations are known to heavily depend on initial conditions [7], so that such a result is not general, but is dependent on the seismic history and any historical foundation deformations at a particular site.

3.3 Effect of adding a heavier neighbouring structure of the same foundation type

This section continues to focus on the behaviour of the lighter structure of the pair tested, but now incorporating the SSSI from the adjacent heavier structure. Peak storey acceleration, cyclic sway and inter-storey drift in each EQ are shown in Figure 12, in which the 1:1 dividing line indicates parity. The maximum inter-storey drift here was around 6.5 mm (0.2% of storey height), which was under the 'no damage' limit of 0.4% for buildings having brittle non-structural elements in EC8 indicating that all of the structures performed elastically during the tests, and the use of an elastic structural physical model was justified.

Considering the isolated structures first, Figure 12 demonstrates that in terms of inter-storey drift (the part which induces bending within the columns) rafts and strips gave very similar response for all earthquakes, even though the severity of liquefaction was different. The sway was lower in the strip cases however, implying that the reduced storey accelerations in these cases were associated with less cyclic rocking in the structures (see Figure 13(a)). This may initially appear counter-intuitive as the rafts would be expected to have had a higher rotational foundation stiffness than the strips; however, due to the higher bearing pressures acting on the strips (lower FOS, Table 2) uplift was easier in the raft case than the strip case.

While strips and rafts saw similar structural response in terms of column deformation in the isolated structure case for all earthquakes, SSSI resulted in a significant reduction in structural response in the raft cases and a slight increase in response for the strip cases for all measures of structural response, including inter-storey drift. To investigate this further, transfer functions for the structure of interest (using the accelerometer data between the foundation and storey 1) were determined during each EQ for all cases. A single-degree-of-freedom response curve for magnitude of response was used to determine the best-fit fundamental natural period T_{n} and equivalent viscous damping ratio ξ (results shown in Figure 14):

$$\left|\frac{\ddot{x}}{\ddot{y}}\right| = \sqrt{\frac{1 + (2\xi T_n/T)^2}{\left(1 - (T_n/T)^2\right)^2 + (2\xi T_n/T)^2}} \tag{7}$$

where x is the absolute displacement of the first storey; y is the foundation input displacement; T is the base excitation period; and T_n is effective natural period.

The dashed line shown in Figure 14 represents the designed fixed-base natural period of the lighter structure (0.21s). The difference between the isolated data points and this line therefore indicates the effect of SSI in liquefied soil in lengthening the fundamental natural period. The isolated structure with strip foundations exhibited generally higher effective periods than the isolated rafts since the strip foundations had lower stiffness resulting in greater lengthening. The lengthened effective natural period of the structures derived from the transfer functions of all four tests fell within the area of the response spectra where acceleration reduces with period (Figure 4), which explains why the isolated raft cases saw greater peak acceleration (Figure 12(a)). Comparing the isolated and adjacent cases in Figure 14, the structure exhibited a general reduction in period due to SSSI in strip cases (Figure 14(a)) which resulted in increased amplification of storey acceleration. In contrast, for the raft foundations shown in Figure 14(b), the structure had a generally increased effective period resulting in a reduction of structural response. These identified changes in effective period explain the differences between rafts and strips in terms of structural performance in Figure 12(a). Equivalent viscous damping results are shown in Figure 14(c) and (d). In all but one case, the damping was substantially reduced by SSSI. This would suggest that all measures of response should have reduced for both raft and strip cases in Figure 12. Figure 15 explains this combined effect graphically by applying period and damping change on the EQ2 spectra accounting for surface liquefaction (i.e. at Point A) as an example. The structural response of an isolated structure on a raft foundation was generally reduced by SSSI because the reduction caused by the period lengthening effect outweighed the increase caused by lower damping. In the case of a structure on strip foundations there were combined detrimental effects of both damping reduction and period shortening resulting in an increase in structural response (at least within this descending branch of the spectrum).

The overall (permanent) earthquake-induced post-earthquake tilt (rotation) of all structures is shown in Figure 16. The structure on the raft foundation in the adjacent case was seen to lose its beneficial effects relative to the isolated case due to SSSI but this was no worse than the values observed for either isolated or adjacent strip foundation cases (Figure 16(a)). This greater tilt was consistent with the reduced structural response in raft cases, with greater energy dissipation having occurred in plastic soil deformation protecting the structure. The effect of SSSI on permanent rotations for the strip foundations case was small/negligible, except for EQ5.

The accumulated post EQ settlement is shown in Figure 17 with the free-field settlement derived from the isolated strip case as a reference. The final building settlements in adjacent cases were greater than those in isolated cases, although adjacent structures also had larger initial settlements due to static SSSI. In terms of the earthquake-induced settlement (shown between the dashed lines in Figure 17) the shallow foundations showed smaller co-seismic settlements in the adjacent cases due to SSSI which is consistent with previous observations in non-liquefied soil [7]. In contrast, the raft foundations showed much greater co-seismic settlement in the adjacent case, consistent with greater plastic deformation within the foundation soil. However, as gross settlement is not as damaging as differential movement, and the induced rotation of the raft in the adjacent case was similar to that in the strip case (Figure 16), the protective effect of rafts in reducing structural demand in the adjacent case may outweigh the increased foundation movement. These results suggest that raft foundations are more desirable when used in urban areas in terms of reducing structural demands, though at a cost of greater post-earthquake foundation deformation.

4 Conclusion

This paper has investigated the effects of liquefaction on isolated low-rise structures on strip and raft foundations, and the influence of SSSI on this behaviour when a heavier neighbouring structure of the same foundation type is present, in terms of soil response, structural response and foundation response. It was shown that the soil factor in EC8 describing ground motion amplification (site effect) could reduce significantly due to partial or full liquefaction. The depth of full liquefaction could be estimated using a simple method based on the result of a standard liquefaction susceptibility analysis. It was also possible to estimate an upper bound on the peak r_u-profile with depth using this method, from which the soil factor could be estimated. This finding however requires further research to generalise the result for more soil types/densities and building types. The results of this study suggest that the selection of suitable foundation type can significantly influence the structural and foundation response of buildings. In terms of SSI on liquefiable soil, using strip foundations resulted in lower structural response (isolated structure) although there was a trade-off in terms of increased post-earthquake foundation deformation. When SSSI occurs (i.e. in an urban area where there are closely-spaced adjacent structures) raft foundations resulted in reduced structural demand caused by the combined effects of SSSI-induced period lengthening (in a descending branch of the spectrum) which outweighed the effects of any SSSI-induced reduction in damping. There was again a price to pay in terms of increased post-earthquake foundation deformation. It is suggested that new urban areas might target raft foundations as a way of reducing structural demand. The results also suggest that if adjacent buildings are to be added next to existing structures, it may be beneficial for them to have raft foundations, though further research would be desirable to consider the interaction between adjacent dissimilar foundation types.

5 Acknowledgements

The Authors would like to thank Mark Truswell, Grant Kydd, Willie Henderson and Gary Callon at the University of Dundee for their assistance in making the models and running the centrifuge tests. The authors would also like to thank China Scholarship Council for its financial support of the PhD studies of the first author.

6 Nomenclature

B =width of foundation in prototype

CRR = cyclic resistance ratio

CSR = cyclic stress ratio

EI =bending stiffness

$EPWP$=excess pore water pressure generated in the soil

F_{SL}=factor of safety against liquefaction

FOS =static factor of safety of structure

I_D=relative density

K_1, K_2, K_{eq}=total lateral stiffness of the first storey, total lateral stiffness of the second storey, equivalent lateral stiffness of the structure in the fundamental mode, respectively

L = length of foundation in prototype

M_1, M_2, M_{eq}= total mass of the first storey, total mass of the second storey, equivalent mass of the structure, respectively

N= numbers of stories of structure

$(N_1)_{60}$= normalised SPT blowcount

PGA= peak ground acceleration

r_u , $r_{u,FF}$, $r_{u,predicted}$=excess pore water pressure ratio in general, in free field and predicted through simple prediction method, respectively

S_e, $S_{e,FF\ surface}$, $S_{e,input}$ = response spactra in general, in free field surface and input, respectively

SSI = Soil-structure interaction

SSSI = Structure soil-structure interaction

T = base excitation period, effective natural period, in Equation 7

T_n =natural period of structure, in Equation 2

x =absolute displacement of the first storey

y= foundation input displacement

$\overline{y}_2$, =normalized modal coordinates in the fundamental mode

ξ =equivalent viscous damping ratio

7 Reference list

[1] Celebi M. Seismic responses of two adjacent buildings: Interaction. Journal of Structural Engineering. ASCE 1993; 119 (8): 2477–92.

[2] Luque R, Bray J. Dynamic analyses of two buildings founded on liquefiable soils during the Canterbury earthquake sequence. Journal of Geotechnical and Geoenvironmental Engineering ASCE 2017;143(9): 04017067

[3] Wirgin A, Bard P-Y. Effects of buildings on the duration and amplitude of ground motion in Mexico City. Bulletin of the Seismological Society of America 1996; 86(3):914–920.

[4] Tsogka C, Wirgin A. Simulation of seismic response in an idealized city. Soil Dynamics and Earthquake Engineering 2003; 23 (5), 391–402.

[5] Aldaikh H., Alexander N.A., Ibraim E, Knappett J. A. Shake table testing of the dynamic interaction between two and three adjacent buildings (SSSI). Soil Dynamics and Earthquake Engineering 2016; 89:219–232.

[6] Aldaikh H, Alexander N.A, Ibraim E, Oddbjornsson O. Two dimensional numerical and experimental models for the study of structure–soil–structure interaction involving three buildings. Computers & Structures 2015; 150: 79–91.

[7] Knappett JA, Madden P, Caucis K. Seismic structure–soil–structure interaction between pairs of adjacent building structures. Géotechnique 2015; 65(5): 429–441.

[8] Liu L, Dobry R. Seismic response of shallow foundation on liquefiable sand. Journal of Geotechnical and Geoenvironmental Engineering. ASCE 1997; 123(6): 557-567.

[9] Bertalot D, Brennan AJ. Foundations influence of initial stress distribution on liquefaction-induced settlement of shallow foundations. Géotechnique 2015; 65(5): 418-428.

[10] Muir Wood D. Geotechnical modelling. London UK. Spon Press. Taylor and Francis. 2004.

[11] Iai S, Tobita T, Nakahara T. Generalised scaling relations for dynamic centrifuge tests. Géotechnique 2005; 55(5) 355-362.

[12] Storie BL. Soil-foundation-structure interaction in the earthquake performance of multi- storey buildings on shallow foundations. PhD thesis. University of Auckland. 2016.

[13] Jiang X, Yan Z. Earthquake response analysis of building-foundation-building interaction system. Journal of Vibration Engineering 1998;11(1):31–37.

[14] Yahyai M, Mirtaheri M., Mahoutian M, Daryan AS. Assareh M A. Soil structure interaction between two adjacent buildings under earthquake load. American Journal of Engineering and Applied Sciences 2008; 1(2): 121-125.

[15] Alexander NA, Ibraim E, Aldaikh H. A simple discrete model for interaction of adjacent buildings during earthquakes. Computers and Structures 2013; 124, 1–10.

[16] Knappett JA. and Craig RF. Craig's soil mechanics. 8th edn. London, UK: Spon Press. 2012.

[17] Kumar J, Kouzer KM. Bearing capacity of two interfering footings. International Journal for Numerical and Analytical Methods in Geomechanics 2008; 32:251–264.

[18] Knappett JA, Haigh SK, Madabhushi SPG. Mechanisms of failure for shallow foundations under earthquake loading. Soil Dynamics and Earthquake Engineering 2006; 26. 91-102

[19] NEHRP. Recommended provisions for the development of seismic regulations for new buildings 2003 Edition. Building Seismic Safety Council, Washington, DC.

[20] Schofield AN. Dynamic and earthquake geotechnical centrifuge modelling. International Conferences on Recent Advances in Geotechnical Earthquake Engineering and Soil Dynamics 1981; 2.

[21] Stewart DP, Chen YR, and Kutter BL. Experience with the use of methylcellulose as a viscous pore fluid in centrifuge models. Geotechnical Testing Journal 1998; 21(4), 365–369.

[22] Bertalot D. Foundations on layered liquefiable soils. PhD thesis. University of Dundee. Dundee, UK; 2013.

[23] Bertalot D, Brennan AJ, Knappett JA, Muir Wood D, Villalobos F. A. Use of centrifuge modelling to improve lessons learned from earthquake case histories. Proceedings of the 2nd European conference on physical modelling in geotechnics, Eurofuge 2012. Delft, the Netherlands.

[24] Zeng X, Schofield AN. Design and performance of an equivalent-shear-beam container for earthquake centrifuge modelling. Géotechnique 1996; 46(1), 83–102.

[25] Madabhushi SPG, Teymur B. Experimental study of boundary effects in dynamic centrifuge modelling. Géotechnique 2003; 53(7), 655–663.

[26] Lee S. H, Choo YW, Kim DS. Performance of an equivalent shear beam (ESB) model container for dynamic geotechnical centrifuge tests. Soil Dynamics and Earthquake Engineering. 2013; 44, 102–114.

[27] Lauder K. The performance of pipeline ploughs. PhD thesis. University of Dundee. Dundee, UK; 2011.

[28] BSI. BS EN 1998-1:2005: Eurocode 8: Design of structures for earthquake resistance – Part 1: General rules, seismic actions and rules for buildings. British Standards Institution. London, UK; 2005.

[29] Brennan AJ, Knappett JA, Bertalot D, Loli M, Anastasopoulos I, Brown MJ. Dynamic centrifuge modelling facilities at the University of Dundee and their application to studying seismic case histories. In Proceedings of the 8th international conference on physical modelling in geotechnics (eds C. Gaudin and D. J. White), 227–233. London, UK: Taylor & Francis Group.

[30] Idriss IM, Boulanger RW. SPT Based Liquefaction Triggering Procedures. Report No. UCD/CGM-10-02, Centre for Geotechnical Modelling, Department of Civil and Environmental Engineering, University of California Davis, California; 2010.

[31] Skempton AW. Standard penetration test procedures and the effects in sands of overburden pressure, relative density, particle size, ageing and overconsolidation. Géotechnique 1986; 36(3), 425–447.

[32] Madabhushi G, Knappett AJ, Haigh S. Design of pile foundations in liquefiable soils. Imperial College Press, London, UK. 2010.

[33] Loli M, Knappett JA, Brown MJ, Anastasopoulos I, Gazetas G. Centrifuge modeling of rocking-isolated inelastic RC bridge piers. Earthquake Engineering and Structural Dynamics 2014; 43(15): 2341-2359.

List of figure captions

Figure 1 Strip model structure: dimensions at prototype scale are shown in m; dimensions at model scale are given in mm in brackets ().

Figure 2 Test configuration and instrument positions – examples of tests SQ04 and SQ07 shown; dimensions at prototype scale are shown in m; dimensions at model scale are given in mm in brackets ().

Figure 3 Input motion spectra for nominal 5% structural damping.

Figure 4 Normalised input spectra from all tests and a total of twenty events showing ground motion repeatability.

Figure 5 (a) Liquefaction susceptibility F_{SL} and predicted excess pore water pressure ratio $r_{u,predicted}$; (b) measured $r_{u,FF}$ in the free-field along depth in all tests.

Figure 6 Acceleration response spectra of the motion at the free-field soil surface compared to the input ('bedrock') motion showing liquefaction effects (test SQ03 only shown for clarity).

Figure 7 PGA change with depth due to liquefaction effect in the isolated strip case (test SQ03).

Figure 8 Spectral reduction factor along period in the isolated strip case (test SQ03).

Figure 9 Soil factor (free-field amplification) as a function of degree of liquefaction.

Figure 10 Response history of isolated structures during Earthquake 1 (a) Storey 1 acceleration; (b) post EQ settlement; (c) overall tilt; (d) pore pressure ratio of free-field surface; (e) Input motion.

Figure 11 Response history of isolated structures during Earthquake 5 (a) Storey 1 acceleration; (b) post EQ settlement; (c) overall tilt; (d) pore pressure ratio of free-field surface; (e) Input motion.

Figure 12 Structural response of isolated and adjacent cases at storey 1: (a) storey acceleration; (b) cyclic sway and inter-storey drift.

Figure 13 Vertical peak cyclic displacements of the foundations (a) isolated cases; (b) adjacent cases.

Figure 14 Transfer function results: (a) effective period for strip cases; (b) effective period for raft cases; (c) effective damping for strip cases; (d) effective damping for raft cases.

Figure 15 Effects of SSSI on damping and period of isolated relative (EQ2 spectra shown with full liquefaction).

Figure 16 Earthquake induced accumulative rotation (a) for strip cases; (b) for raft cases.

Figure 17 Earthquake induced accumulative settlement (a) for strip cases; (b) for raft cases.

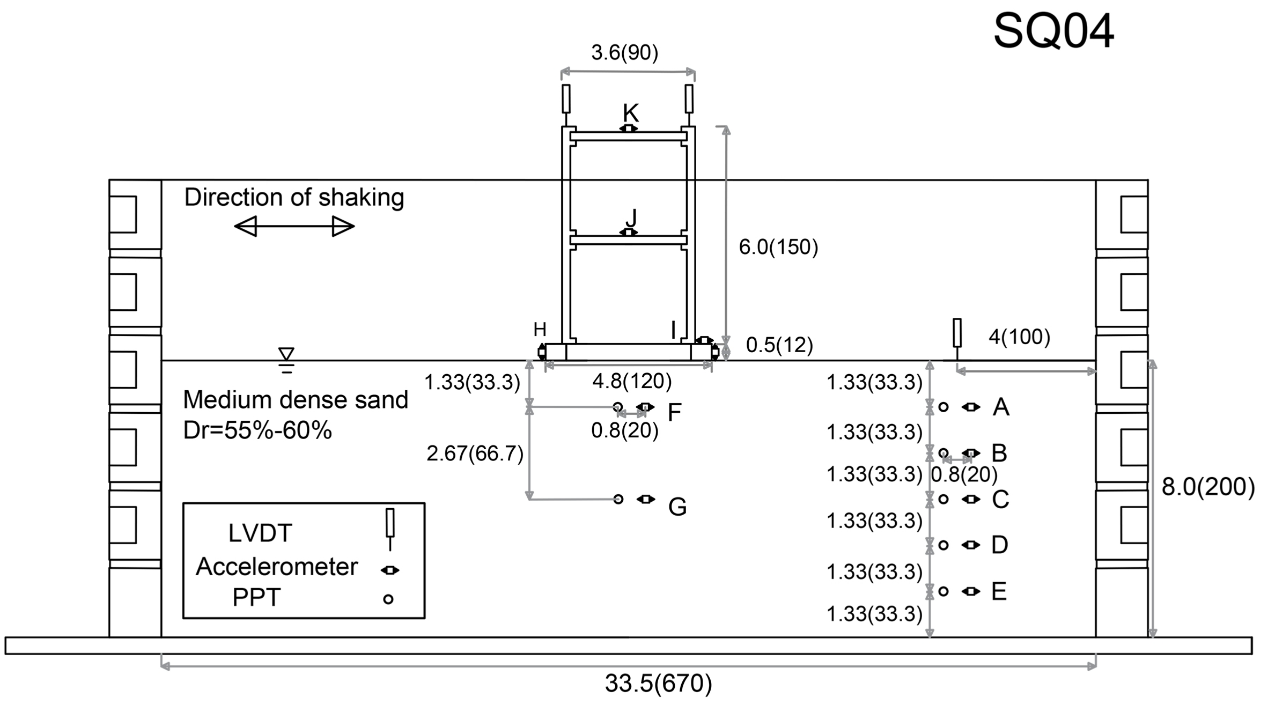

SQ04
3.6(90)
K
J
Direction of shaking
6.0(150)
H
I
0.5(12)
4(100)
1.33(33.3)
4.8(120)
1.33(33.3)
Medium dense sand
Dr=55%-60%
F
A
0.8(20)
1.33(33.3)
2.67(66.7)
B
1.33(33.3)
0.8(20)
G
C
8.0(200)
1.33(33.3)
LVDT
D
Accelerometer
1.33(33.3)
PPT
E
1.33(33.3)
33.5(670)

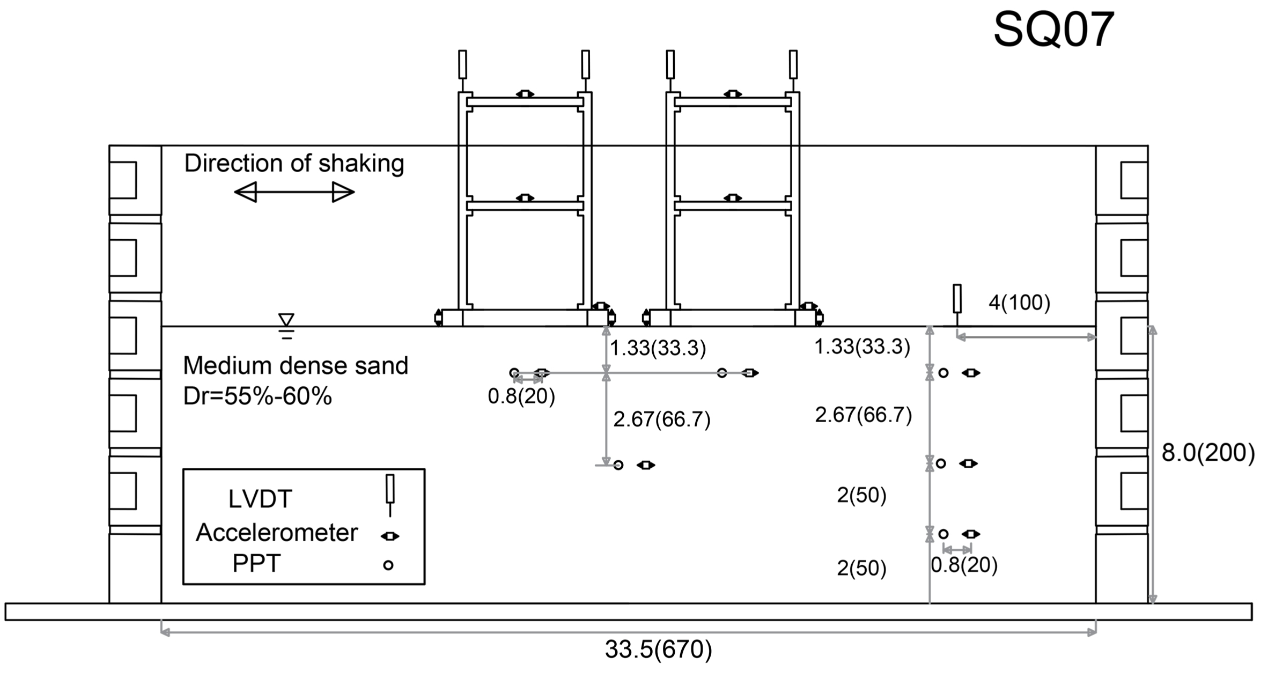

SQ07
Direction of shaking
4(100)
1.33(33.3)
1.33(33.3)
Medium dense sand
Dr=55%-60%
0.8(20)
2.67(66.7)
2.67(66.7)
8.0(200)
LVDT
2(50)
Accelerometer
PPT
2(50)
0.8(20)
33.5(670)

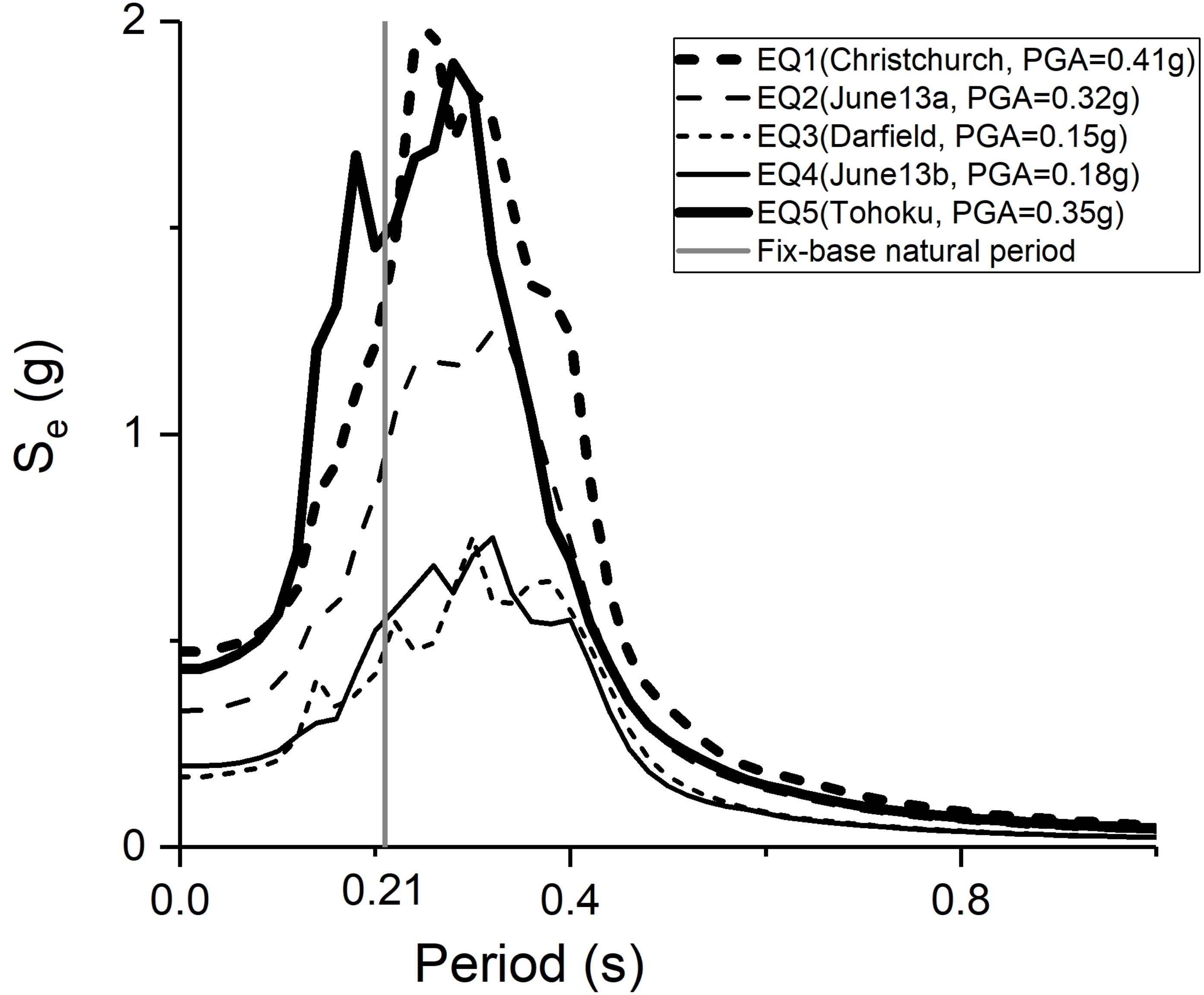

2
1
0
S_e (g)
0.0
0.21
0.4
0.8
Period (s)
EQ1(Christchurch, PGA=0.41g)
EQ2(June13a, PGA=0.32g)
EQ3(Darfield, PGA=0.15g)
EQ4(June13b, PGA=0.18g)
EQ5(Tohoku, PGA=0.35g)
Fix-base natural period

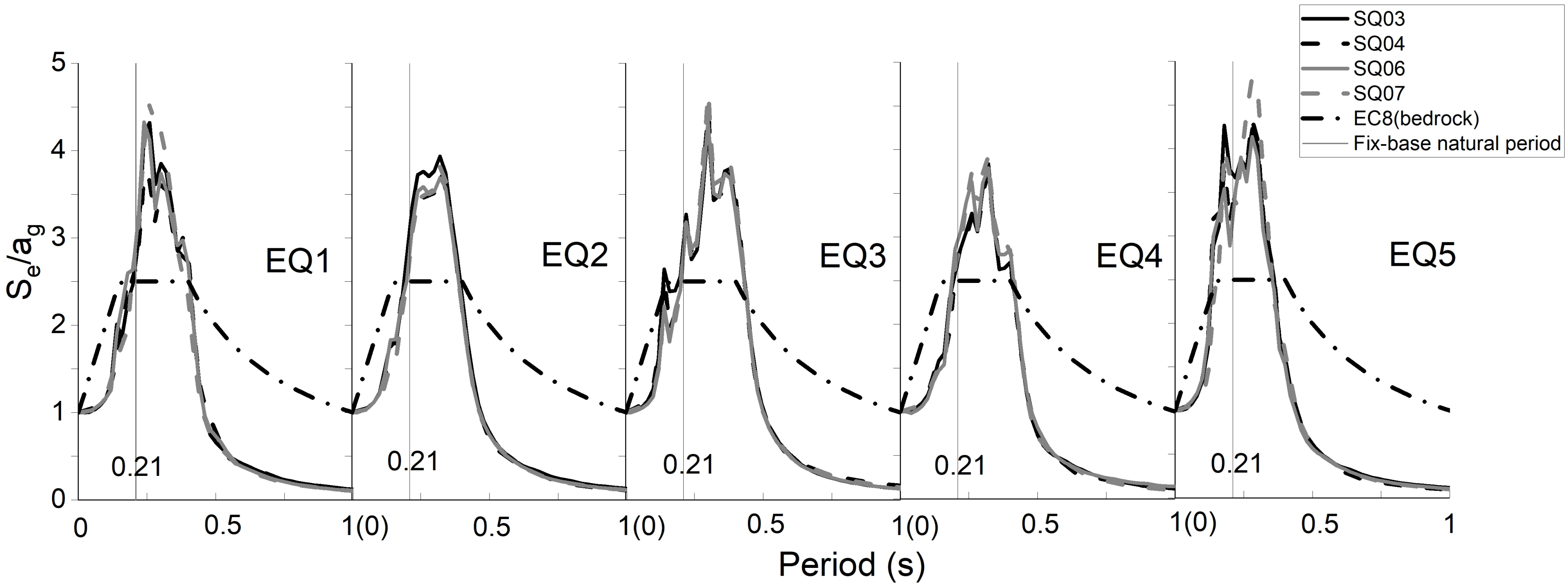

SQ03
SQ04
SQ06
SQ07
EC8(bedrock)
Fix-base natural period
EQ1
EQ2
EQ3
EQ4
EQ5
0.21
Se/ag
Period (s)
0
1
2
3
4
5
0.5
1(0)
1

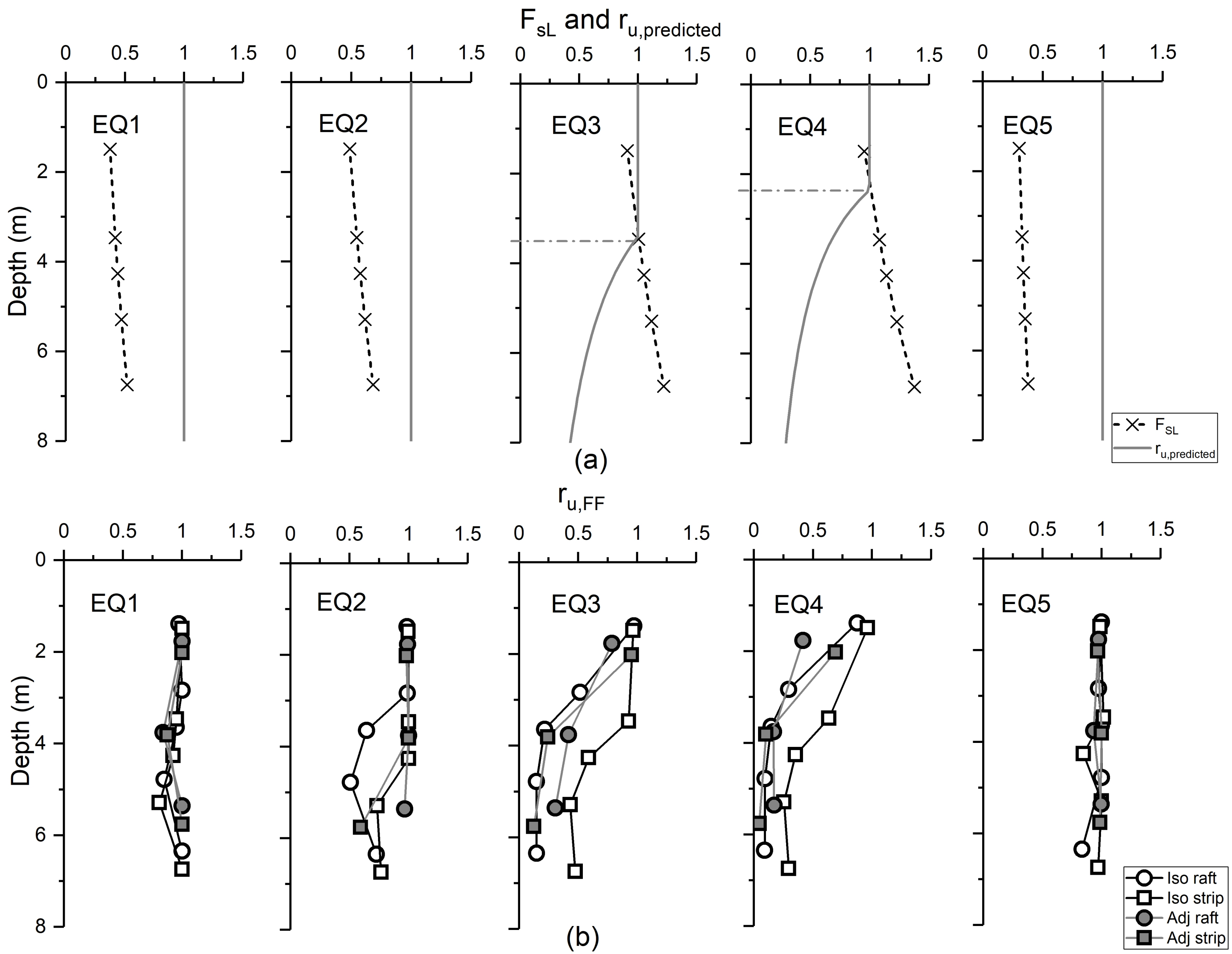

F_{sL} and $r_{u,predicted}$
EQ1
EQ2
EQ3
EQ4
EQ5
Depth (m)
F_{SL}
$r_{u,predicted}$
(a)
$r_{u,FF}$
Iso raft
Iso strip
Adj raft
Adj strip
(b)

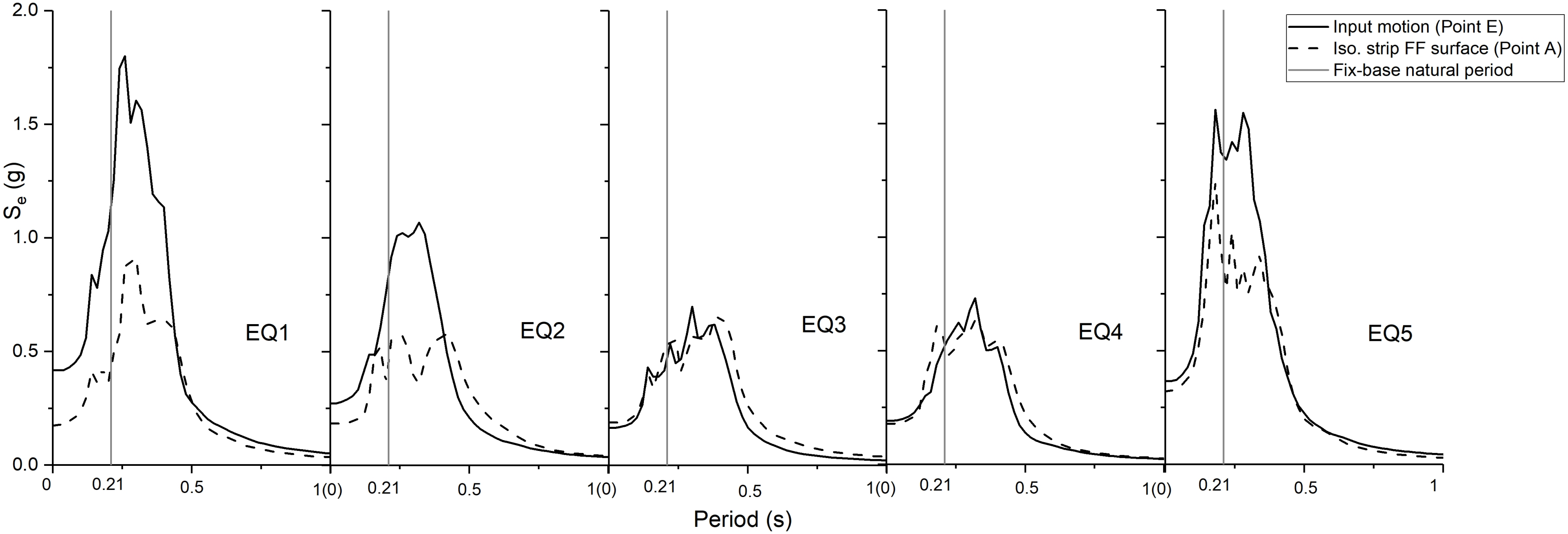

2.0
1.5
1.0
0.5
0.0
S_e (g)
EQ1
EQ2
EQ3
EQ4
EQ5
Input motion (Point E)
Iso. strip FF surface (Point A)
Fix-base natural period
0
0.21
0.5
1(0)
1
Period (s)

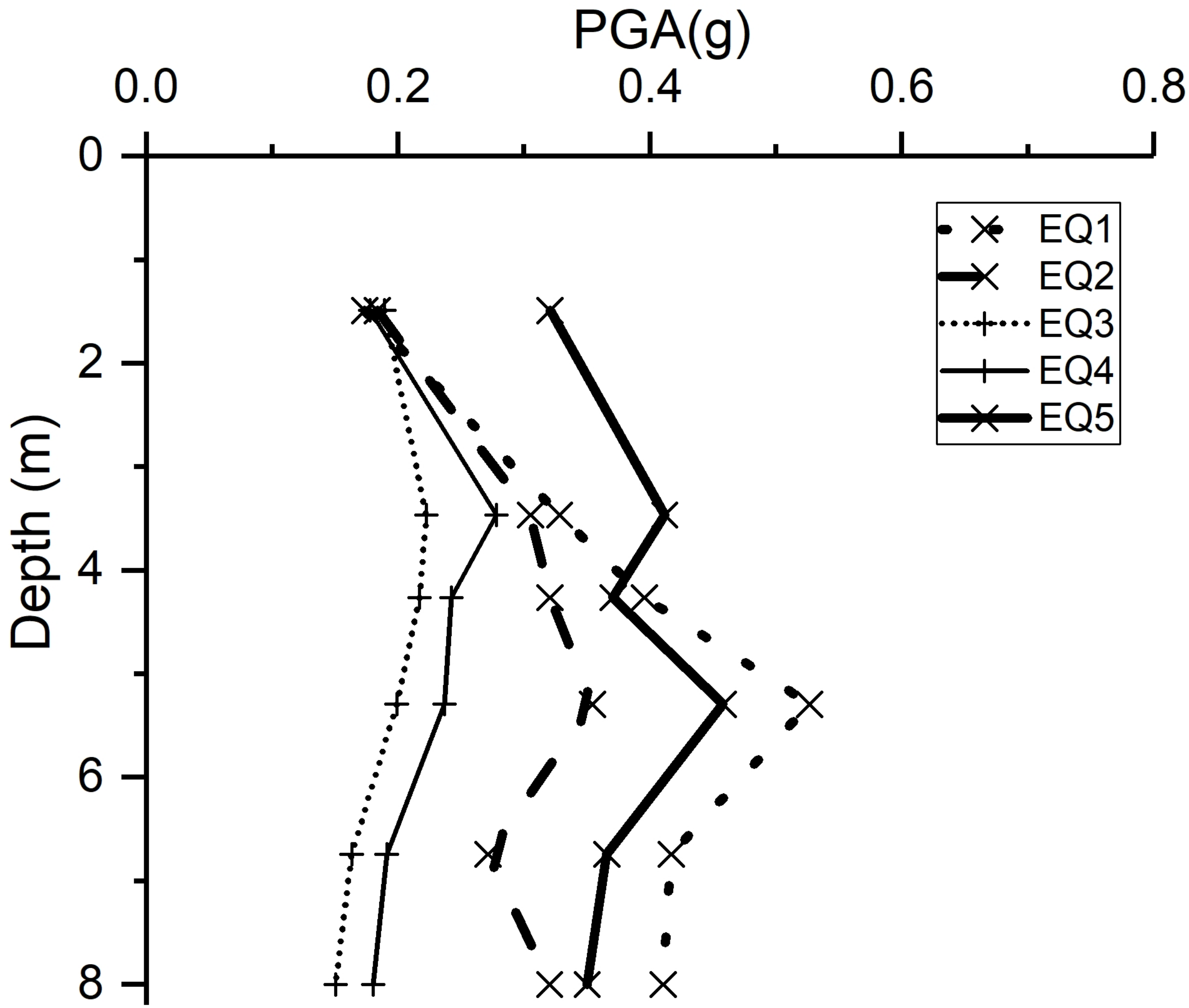

PGA(g)
0.0
0.2
0.4
0.6
0.8
0
2
4
6
8
Depth (m)
EQ1
EQ2
EQ3
EQ4
EQ5

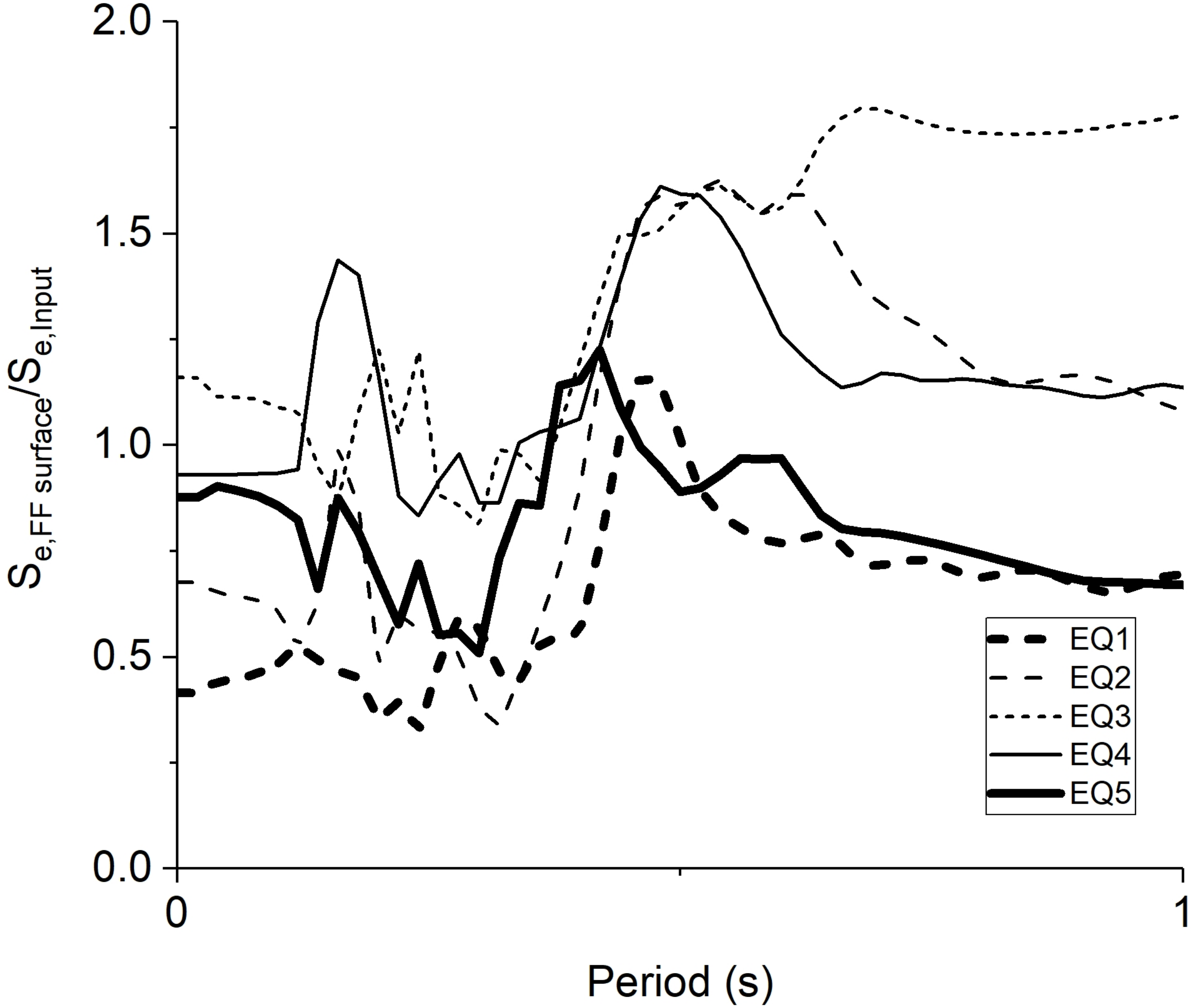

2.0
1.5
1.0
0.5
0.0
0
1
Period (s)
$S_{e,FF\ surface}/S_{e,Input}$
EQ1
EQ2
EQ3
EQ4
EQ5

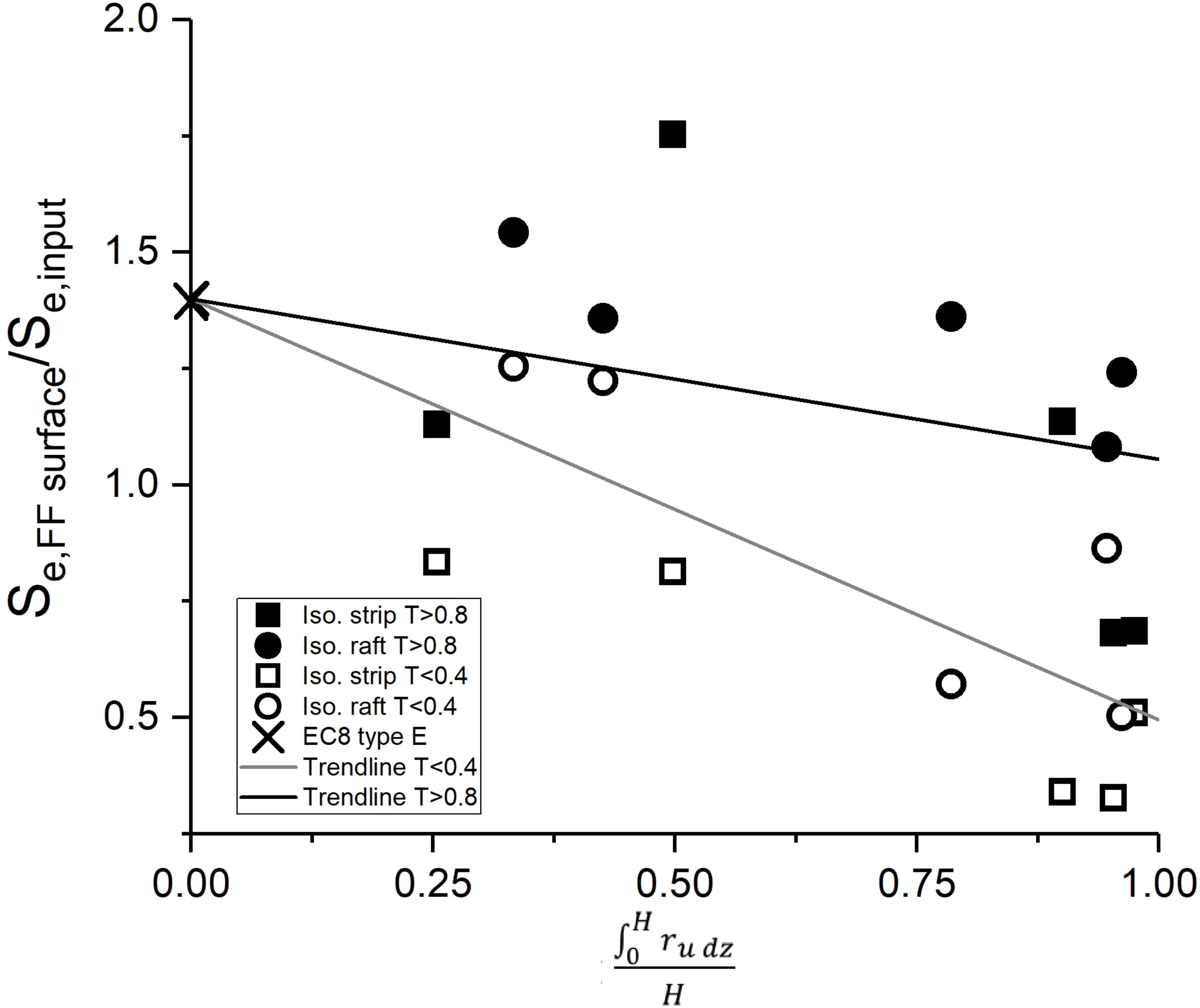

$S_{e,FF\ surface}/S_{e,input}$
2.0
1.5
1.0
0.5
0.00
0.25
0.50
0.75
1.00
$\frac{\int_0^H r_{u\,dz}}{H}$
Iso. strip T>0.8
Iso. raft T>0.8
Iso. strip T<0.4
Iso. raft T<0.4
EC8 type E
Trendline T<0.4
Trendline T>0.8

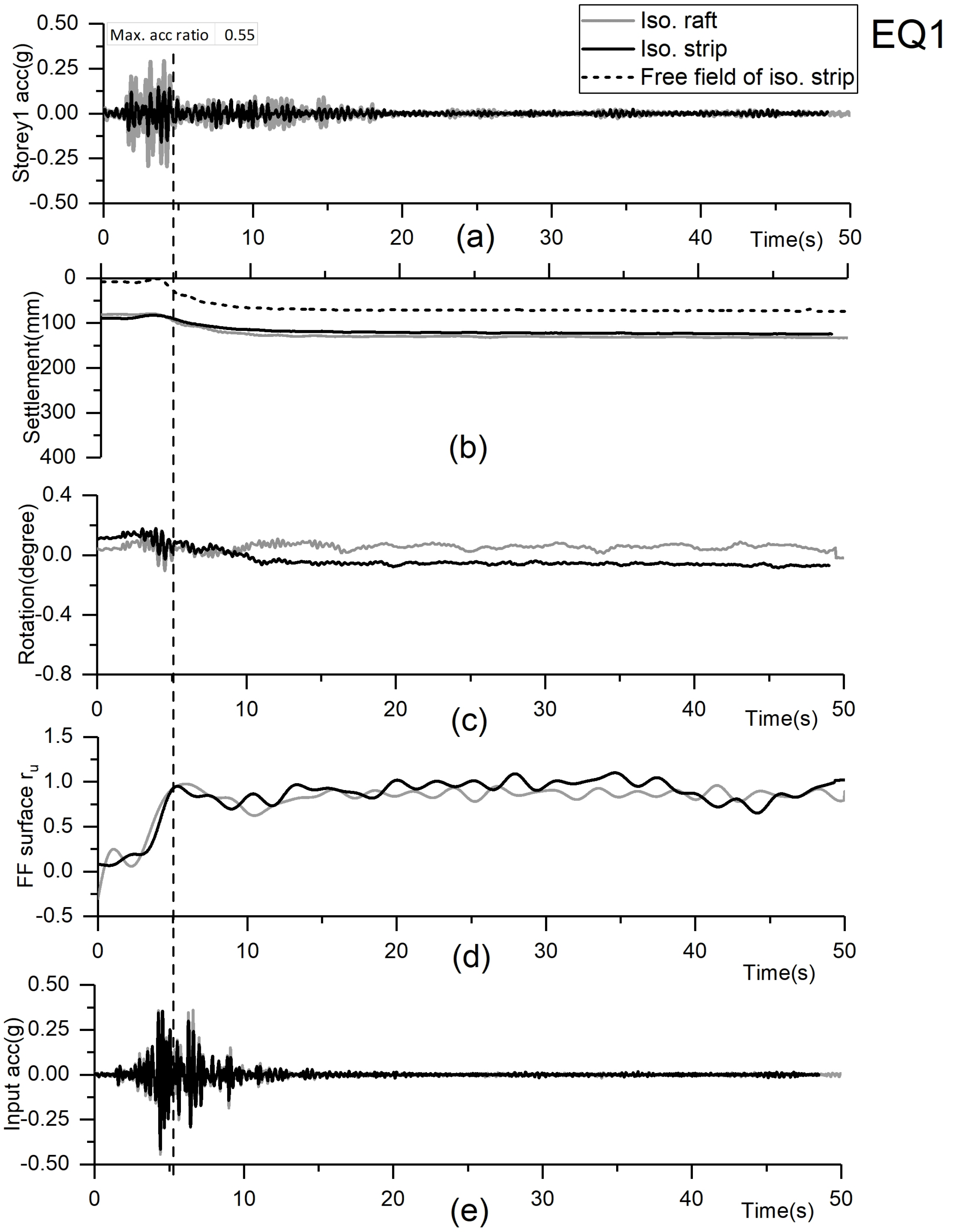

Iso. raft
Iso. strip
Free field of iso. strip
EQ1
Max. acc ratio 0.55
Storey1 acc(g)
(a)
Time(s)
Settlement(mm)
(b)
Rotation(degree)
(c)
Time(s)
FF surface r_u
(d)
Time(s)
Input acc(g)
(e)
Time(s)

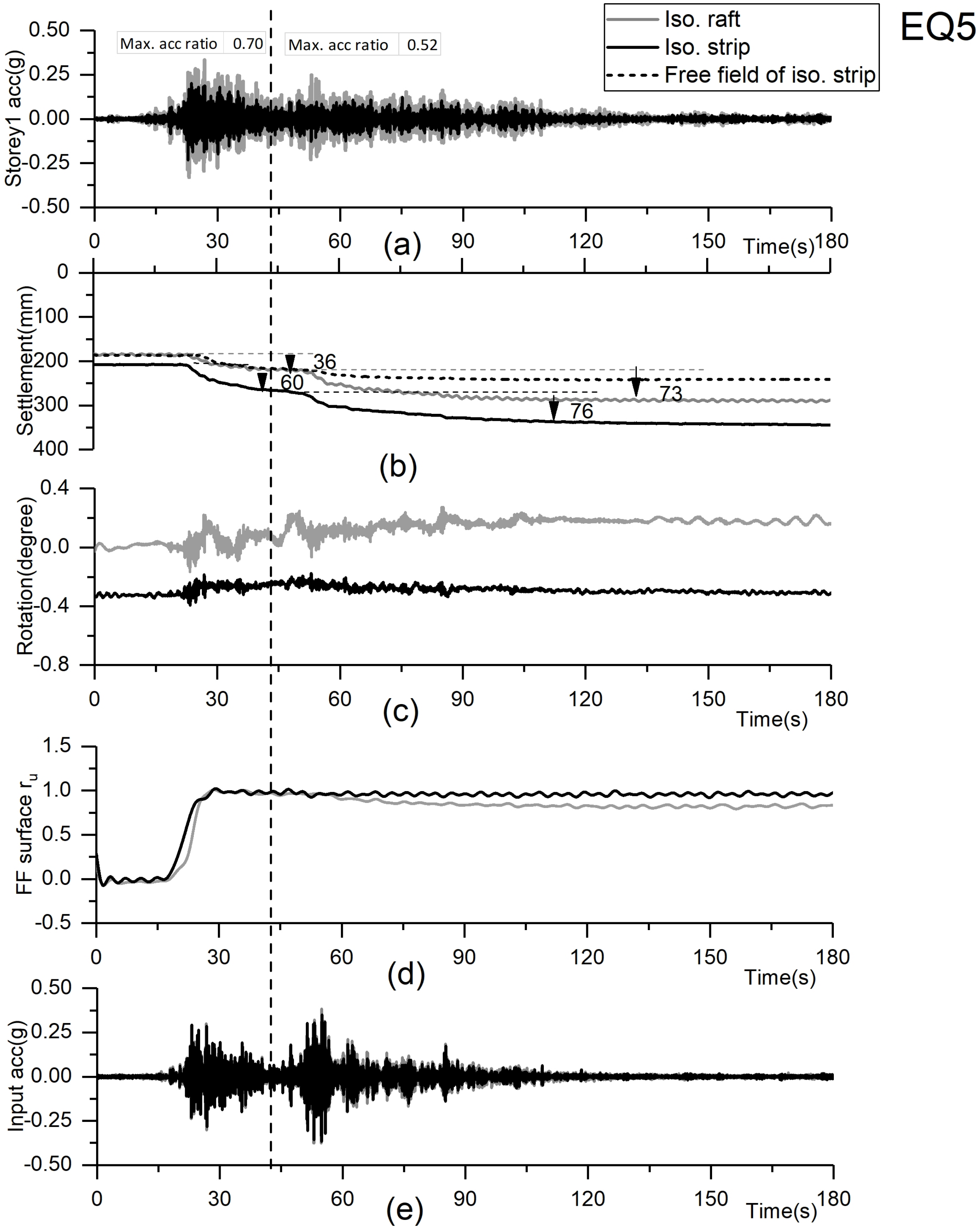
EQ5
Iso. raft
Iso. strip
Free field of iso. strip
Max. acc ratio 0.70
Max. acc ratio 0.52
Storey1 acc(g)
Time(s)
(a)
Settlement(mm)
36
60
73
76
(b)
Rotation(degree)
(c)
FF surface r_u
(d)
Input acc(g)
(e)

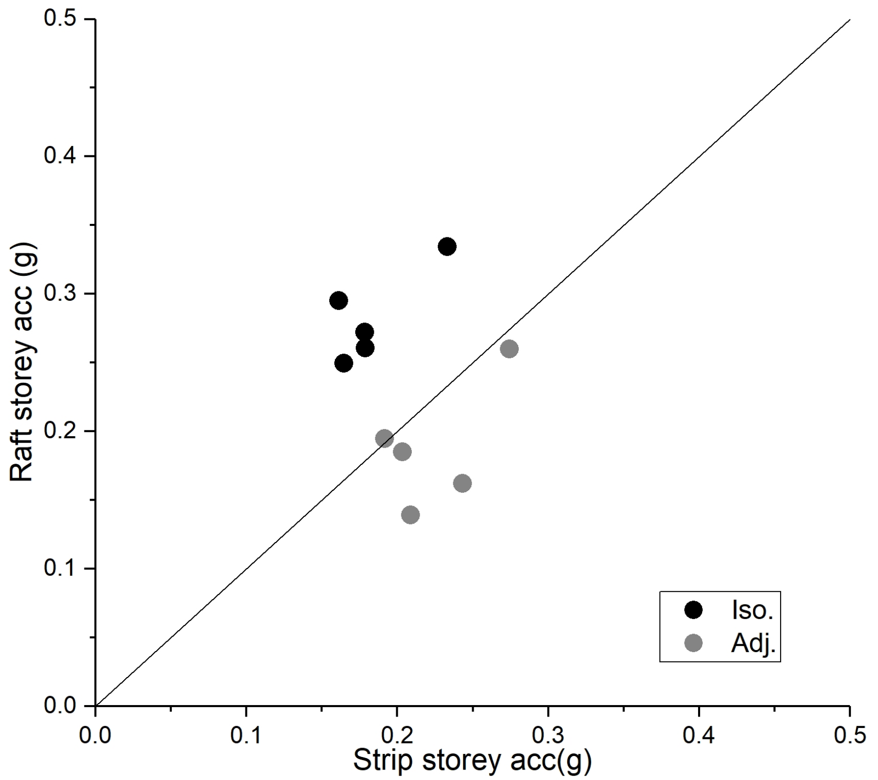

Raft storey acc (g)
Strip storey acc(g)
0.0
0.1
0.2
0.3
0.4
0.5
Iso.
Adj.

(a)

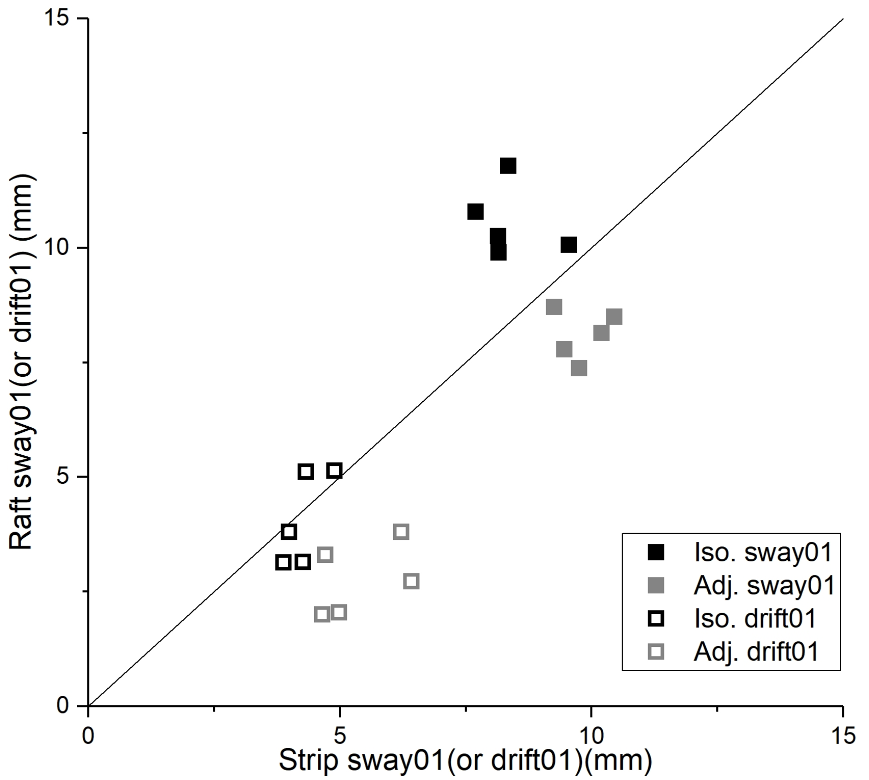

Raft sway01(or drift01) (mm)
Strip sway01(or drift01)(mm)
0
5
10
15
Iso. sway01
Adj. sway01
Iso. drift01
Adj. drift01

(b)

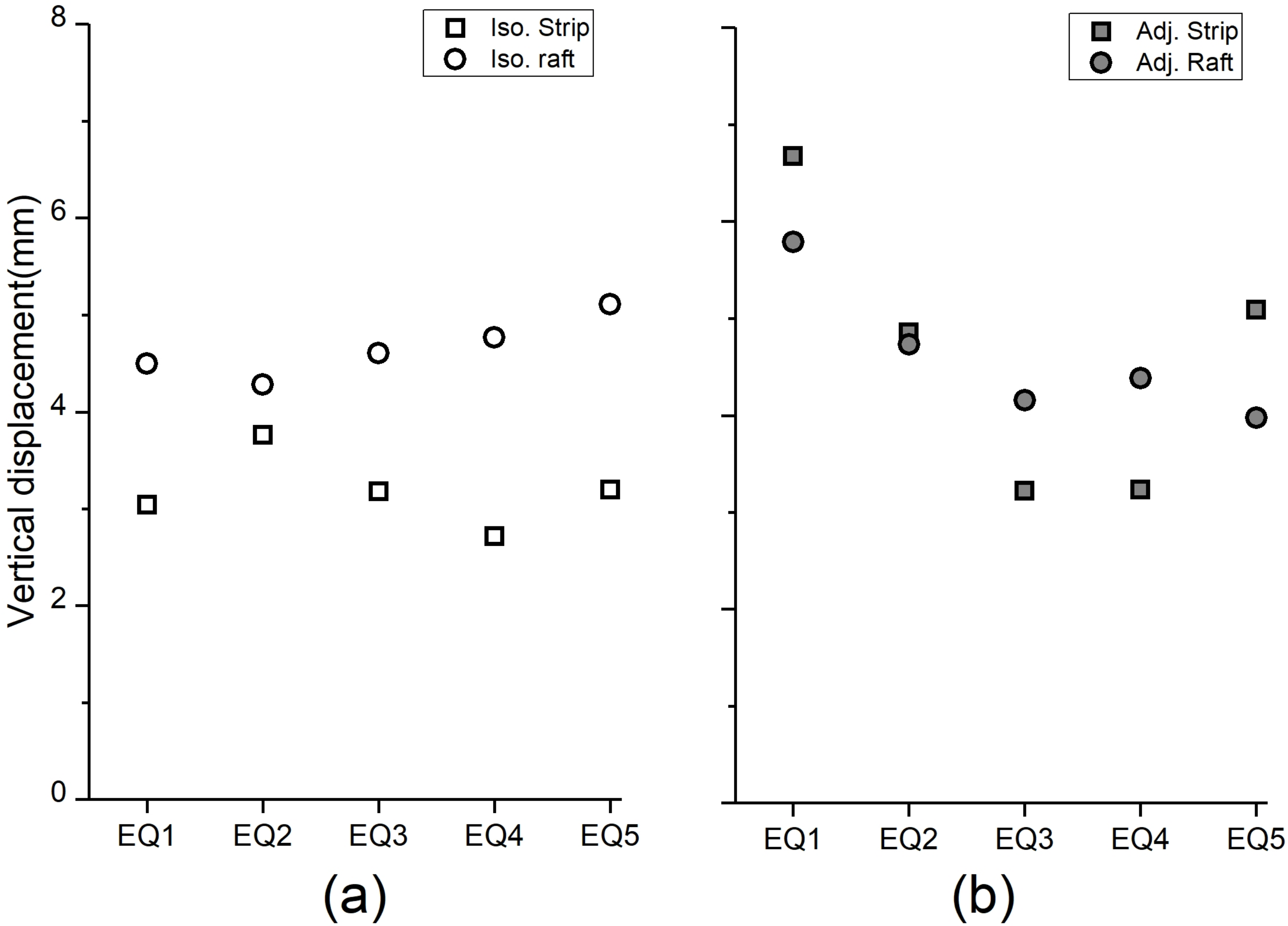

Iso. Strip
Iso. raft
Adj. Strip
Adj. Raft
Vertical displacement(mm)
0
2
4
6
8
EQ1
EQ2
EQ3
EQ4
EQ5
(a)
(b)

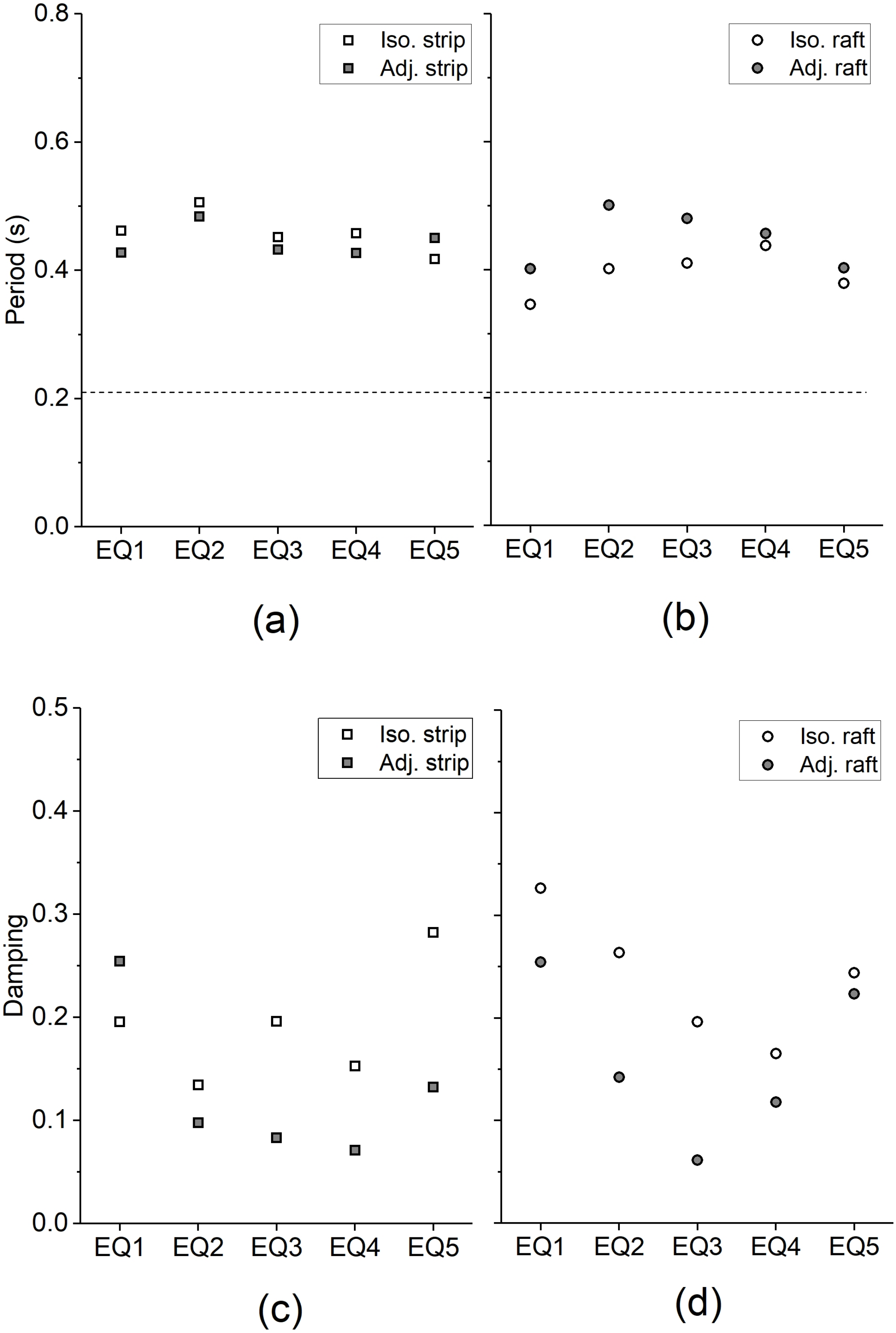

Period (s)
0.0
0.2
0.4
0.6
0.8
Iso. strip
Adj. strip
Iso. raft
Adj. raft
EQ1
EQ2
EQ3
EQ4
EQ5
(a)
(b)
Damping
0.0
0.1
0.2
0.3
0.4
0.5
(c)
(d)

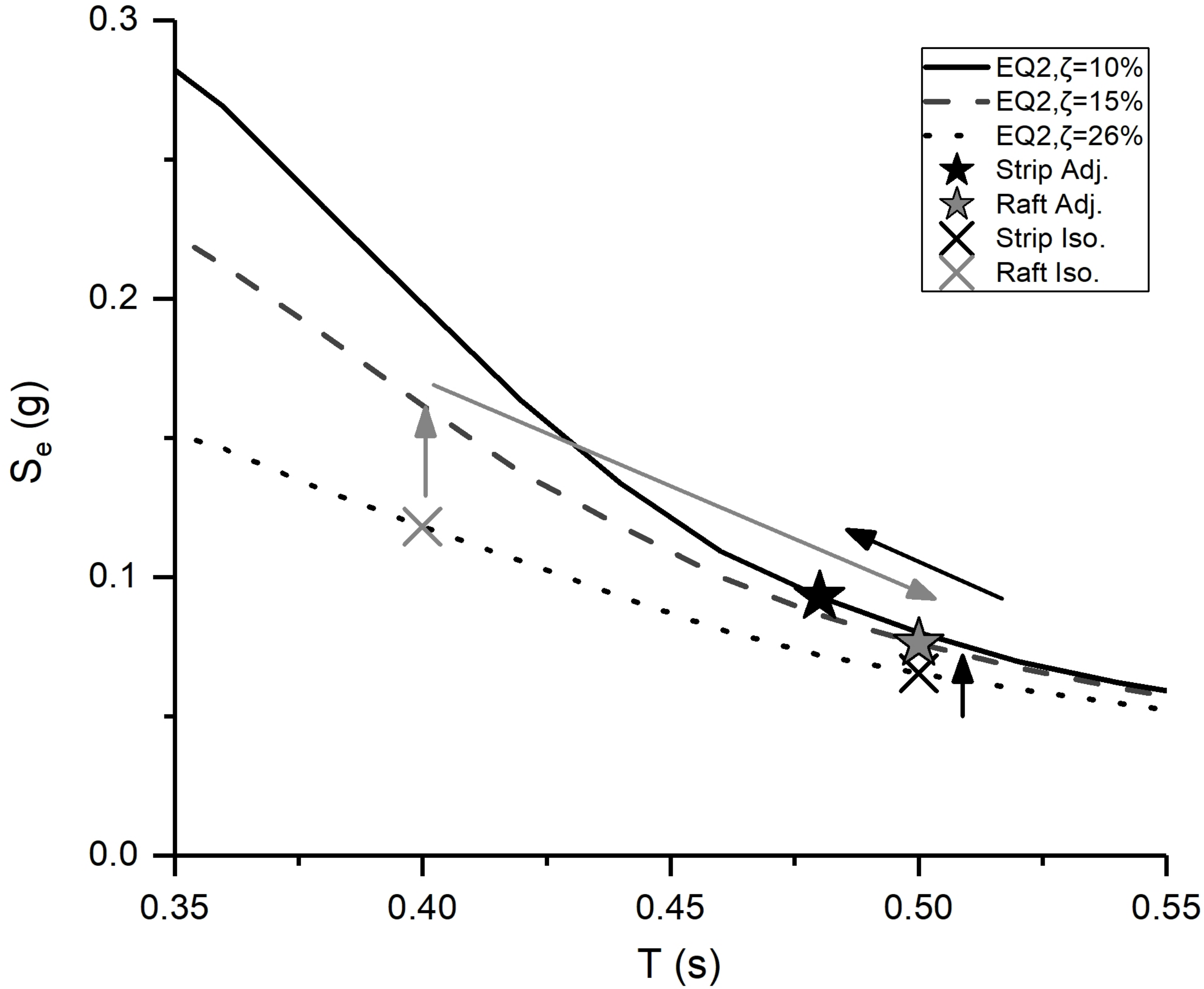

0.3
0.2
0.1
0.0
0.35
0.40
0.45
0.50
0.55
T (s)
S_e (g)
EQ2,ζ=10%
EQ2,ζ=15%
EQ2,ζ=26%
Strip Adj.
Raft Adj.
Strip Iso.
Raft Iso.

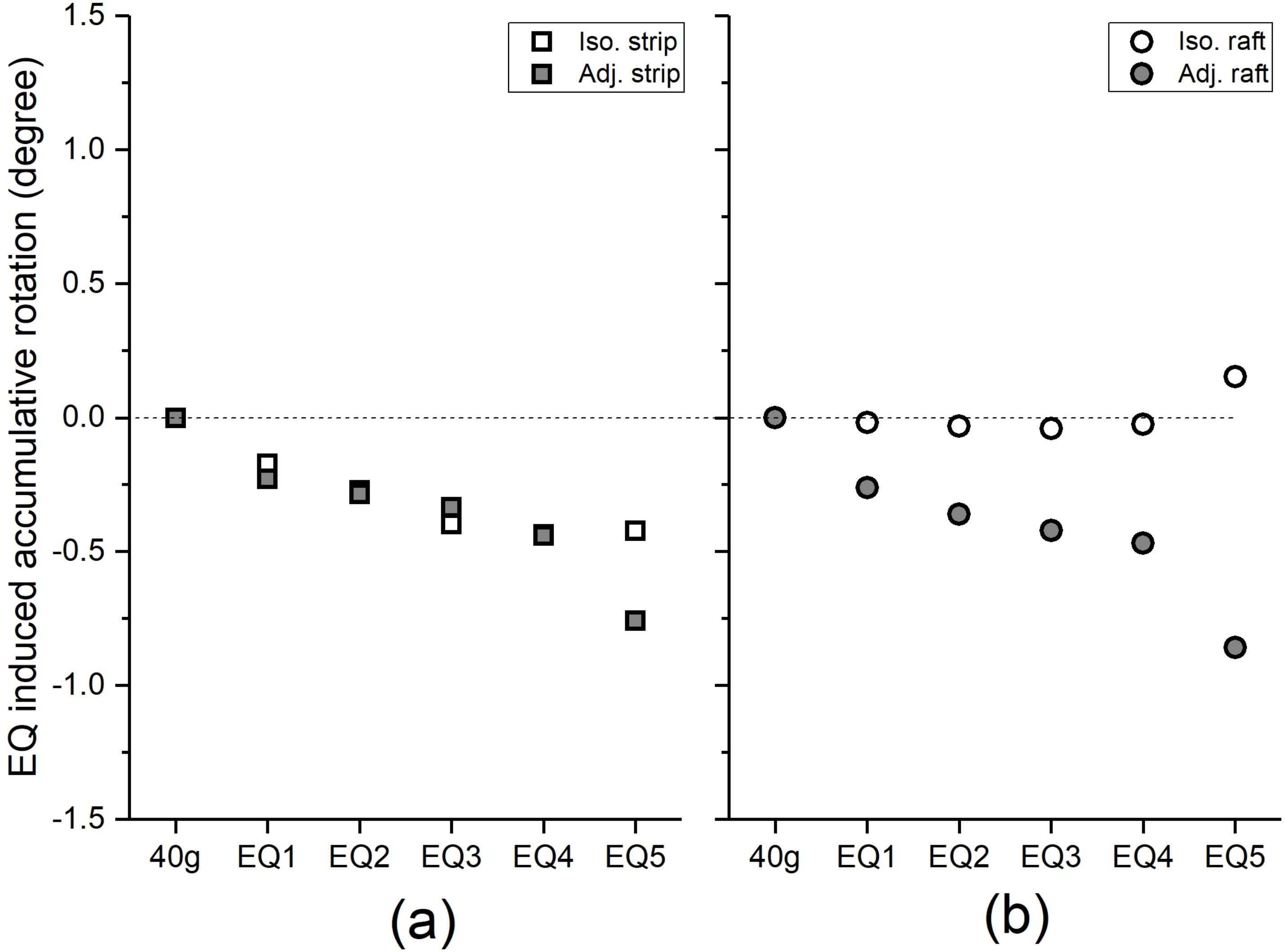

EQ induced accumulative rotation (degree)
1.5
1.0
0.5
0.0
-0.5
-1.0
-1.5
Iso. strip
Adj. strip
40g
EQ1
EQ2
EQ3
EQ4
EQ5
(a)
Iso. raft
Adj. raft
40g
EQ1
EQ2
EQ3
EQ4
EQ5
(b)

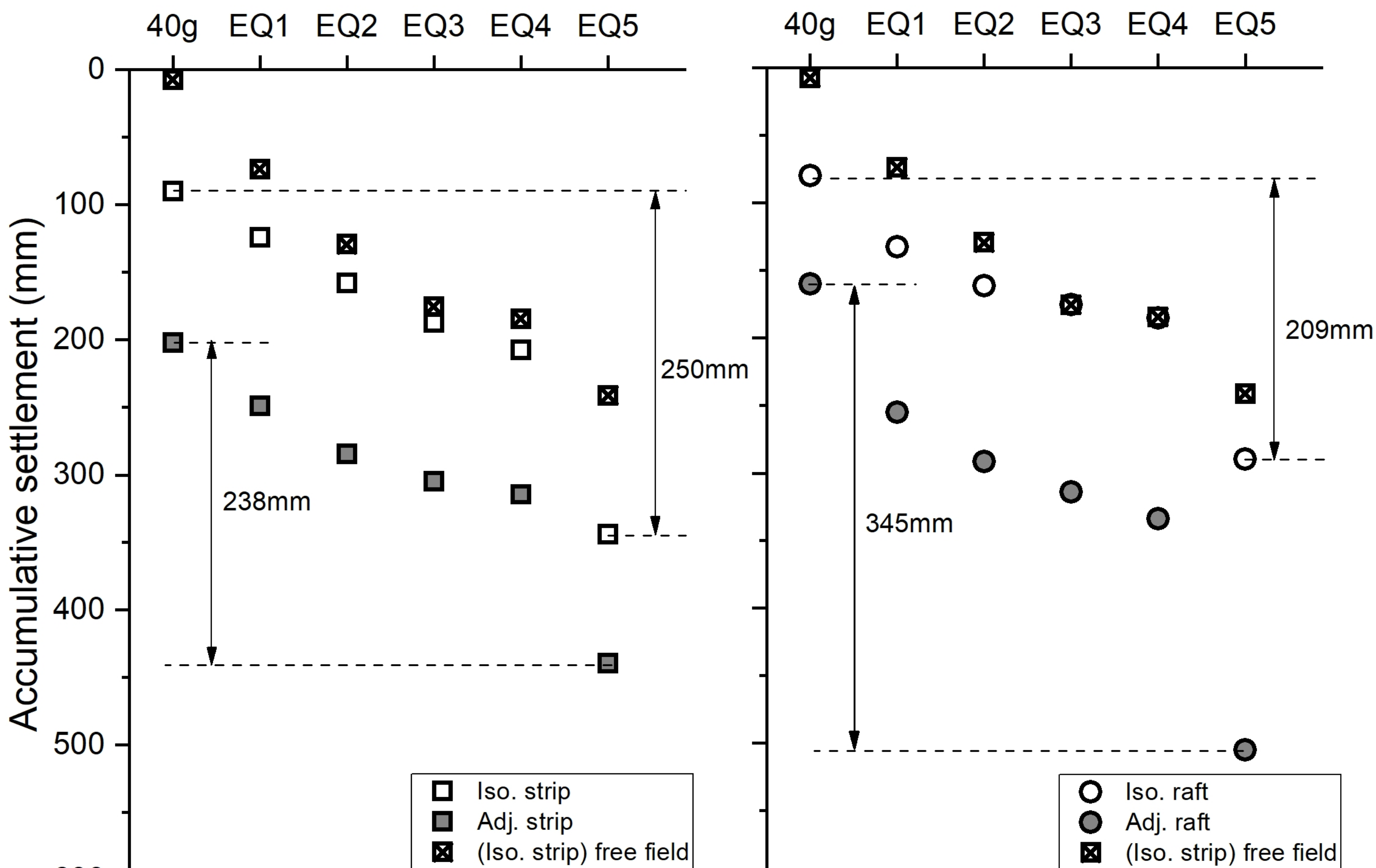

40g
EQ1
EQ2
EQ3
EQ4
EQ5
Accumulative settlement (mm)
0
100
200
300
400
500
600
250mm
238mm
Iso. strip
Adj. strip
(Iso. strip) free field
209mm
345mm
Iso. raft
Adj. raft
(Iso. strip) free field

(a)

(b)

Table 1 Centrifuge test configurations.

Test No.	Configuration	Foundation type	Foundation edge-to edge spacing(m)
SQ03	Isolated, light	Strip	N/A
SQ04	Isolated, light	Raft	N/A
SQ06	Adjacent, light+heavy	Strip, Strip	1.2
SQ07	Adjacent, light+heavy	Raft, Raft	1.2

Table 2 Properties of model structures (at prototype scale).

Parameter: units	structure of interest (Light structure)	accompany structure (Heavy structure)
Storey height: m	3	
Total height: m	6	
Concrete slab dimensions: m	3.6×3.6×0.5	
M_{eq}: kg	16.5×10^3	23.8×10^3
K_{eq}: N/m	37.1×10^6	
Stiffness of columns, *EI*: MNm^2	20.9	
Static *FOS*	3 (strip), 14.7 (raft)	2.5 (strip), 12.2 (raft)
Bearing pressure: kPa	50 (strip), 31 (raft)	62 (strip), 38 (raft)
Fixed-base natural period: s	0.21	0.25
Strip footing spacing (centre-to-centre): m	3.6	

Table 3 Properties of HST95 Congleton sand (after Lauder, 2011).

Property: units	Value
Specific gravity, G_s	2.63
D_{10}: mm	0.09
C_u (uniformity)and C_z (curvature)	1.9 and 1.06
e_{max} and e_{min}	0.769 and 0.467
ϕ'_{pk} at I_D = 55%: °	38
ϕ_{crit}: °	32